
This is the **accepted version** of the journal article:

Adarsh, Nayarassery N.; Novio Vázquez, Fernando; Ruiz-Molina, Daniel. «Coordination polymers built from 1,4-bis(imidazol-1-ylmethyl)benzene : from crystalline to amorphous». Dalton transactions, Vol. 45, issue 28 (July 2016), p. 11233-11255. DOI 10.1039/c6dt01157h

This version is available at <https://ddd.uab.cat/record/282566>

under the terms of the  **CC BY-NC-ND** license

Coordination polymers built from 1,4-bis(imidazol-1-yl-methyl)benzene: From Crystalline to Amorphous

N. N. Adarsh,* Fernando Novio and Daniel Ruiz-Molina

Supramolecular chemistry of bis-imidazole ligand namely 1,4-bis(imidazol-1-yl-methyl)benzene, popularly known as **bix** was explored by various researchers to synthesize functional coordination polymers (CPs). The flexibility of the **bix** ligand, its unpredictable conformation and coordination behaviour with transition metal ions resulted in a huge number of structurally diverse and functionally intriguing CPs. In this perspective review we discuss the progress of CPs of **bix** from crystalline to amorphous materials, since 1997 to current date. More precisely this review emphasize the developments of functional supramolecular coordination polymers from crystalline materials to amorphous nanomaterials built from **bix** ligand.

1. Introduction

Supramolecular chemistry, most popular known as “the chemistry beyond the molecule” has been exploited as one of the main stream research topics in chemistry during last 30 years. From seminal studies in the host-guest molecular assemblies by Cram, Lehn and Pedersen (Nobel Prize in Chemistry in 1987),¹ an exponential emergence of supramolecular materials has had a profound effect on how efficiently chemists prepare structures of different sizes and shapes using spontaneous secondary interactions. Non-covalent interactions such as hydrogen bonding, π - π stacking, dipole–dipole, van der Waals, hydrophobic interactions, etc., play an important role in assembling the molecules to form a supramolecular entity that might perform many functional properties.² A large number of studies have shown applications of supramolecular materials on molecular recognition,^{3a} catalysis^{3b} and transport processes.^{3c} The self-assembly processes of specific ligands of metal complexes as building blocks into highly organized architectures represents one of the most important topics in supramolecular chemistry.



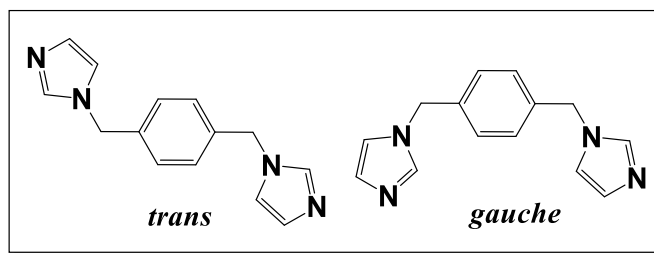
N. N. Adarsh obtained his Master's degree (2004) from SCS, Mahatma Gandhi University, Kerala (India). In 2011, he earned PhD in Chemistry under the supervision of Prof. P. Dastidar in IACS Kolkata, India (affiliated to Jadavpur University). After a few postdoctoral research stays in UCL (Belgium) and Monash University (Australia), he is currently working as a Marie Curie Postdoctoral fellow awarded by EU, in Nanosfun group (ICN2-CSIC, Spain) headed by Prof. D. Ruiz-Molina. His current research interests are coordination and supramolecular chemistry applied to bistable-molecular switch, environmental and nanomedicine.



Fernando Novio received his PhD in chemistry (2007) from the Universitat Autònoma de Barcelona (Spain). After a postdoctoral position in the Laboratoire de Chimie de Coordination at the Université Paul Sabatier (Toulouse, France) working on surface chemistry of metal nanoparticles, he moved in 2011 to the Institut Català de Nanociència i Nanotecnologia (Barcelona, Spain) as senior researcher in the Nanostructured Functional Materials group led by D. Ruiz-Molina. He has initiated different research studies related to the technological and biomedical application of coordination polymer nanoparticles.



Daniel Ruiz-Molina got his PhD on polyradical dendrimers at the Institute of Materials Science of Barcelona (ICMAB). Afterwards he took a postdoctoral position at the UC San Diego working on single-molecule magnets and molecular switches for three years. Since 2001 he got a permanent position at the CSIC. More recently he moved to the new Institut Català de Nanociència i Nanotecnologia (ICN2) where he is leading the Nanostructured Functional Materials group. His main research areas are fabrication of hybrid colloids and surfaces, biomimetic functional nanostructures, coordination polymers and micro-/nanoparticles for smart applications and encapsulation/delivery systems.



Scheme 1: Two plausible conformations of **bix**.

Beyond the supermolecules, the rational combination of metal-organic ligand entities can generate interesting optical, magnetic or catalytic properties, with potential applications. The ligand must contain specific binding sites in a correct arrangement to coordinate the metal ions according to its coordination ability and preferences. The identity of the coordination sites is given by their ability to selectively interact with metal ions having a dominant coordination geometry. Among various organic supramolecular species, imidazole molecule (especially the bis-imidazole ligands) attracted many researchers due to its capability to form novel crystalline organic solids having inclusion or host-guest properties,^{44a} functional coordination polymers (CPs), or metal-organic frameworks (MOFs).^{4b-4e} From the huge amount of reported examples of bis(imidazole) based supramolecular self-assemblies, the ligand 1,4-bis(imidazol-1-yl-methyl)benzene (**bix**) was extensively explored by numerous research groups in the synthesis of functional CPs. The flexibility of the **bix** ligand, its unpredictable conformation and coordination behaviour with transition metal ions resulted in a rich list of structurally diverse and functionally intriguing CPs.

The crystalline structure of **bix** ligand crystallized from water was reported by Robson *et al.* in 1998. The crystals of **bix** belonged to monoclinic $P2_1/n$ space group.⁵ The central aromatic ring of the ligand was positioned at the centre of symmetry and as a result, only half of the ligand was located in the asymmetric unit. The ligand adopted “trans” conformation as depicted in scheme 1. As expected the imidazole moieties of the ligand were found to be nonplanar due to the spacer $-\text{CH}_2-$ and displaying a torsion angle of $\sim 71.59^\circ$ between aromatic ring and imidazole moieties. Crystal structure analysis revealed that the **bix** ligand is involved in hydrogen bonding interaction with the lattice included water molecule and form a 2D hydrogen bonded sheet (Fig. 1).

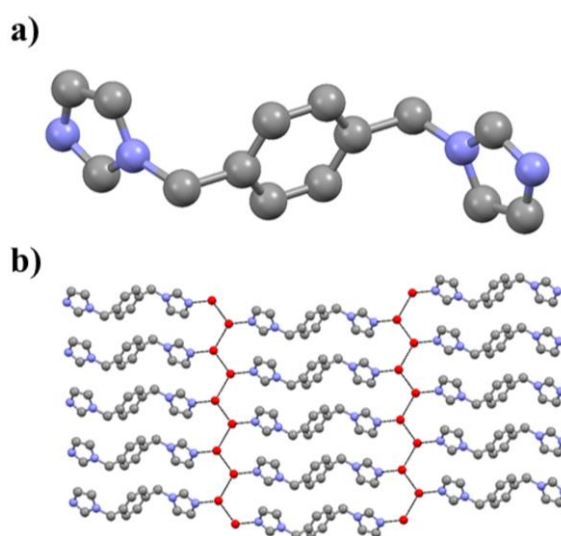


Fig. 1: a) Crystal structure of **bix**; b) 2D hydrogen bonded sheet (water molecules are shown in red balls, hydrogen bondings are shown in black dotted lines).

Bix ligand presents an extraordinary ability to form polymeric networks and to develop secondary interactions which facilitate the formation of extended architectures by supramolecular assemblies. For example Coppens et al. reported a hydrogen bonded porous organic framework obtained by the self-assembly of **bix** and C-methylcalix[4]resorcinarene (CMCR). In the crystal structure, **bix** and CMCR recognize each other via O-H...N hydrogen bonding which resulted in a 1D *zigzag* hydrogen bonded chain. Another 1D *zigzag* chain packed in parallel fashion lead to formation of a double-buckled chain like polymer (Fig. 2a). The overall packing of such chains resulted in a layer motif having porous channels that were occupied by benzil molecules that exhibit luminescence properties (Fig. 2b).⁶ In fact these four benzil molecules are interacting each other by C-H...O and π - π stacking and also involved in various intermolecular interactions with the bix-CMCR host. Such inclusion phenomena resulted in the short life-time of benzil molecule luminescence (580 ns) at 77K compared with free benzil molecule (145 μ s), but nevertheless a behaviour different from that of benzil inclusion compounds with conjugated linkers in which the luminescence was fully quenched.⁷ This differential behaviour can be related to the use of **bix** as non-conjugated spacer with limited flexibility, which allows flexing of the resorcinarene node and retains the required rigidity to produce a large cavity to accommodate the benzil molecules. The **bix** ligand was also explored as guest molecules in supramolecular assemblies of pseudorotaxanes based on β -cyclodextrin,⁸ or pillar[5]arenes,⁹ and as a component in co-crystallization processes;¹⁰ due to its inevitable tendency to be involved in hydrogen bonding and π - π stacking interactions through imidazole moiety and central aromatic backbone.

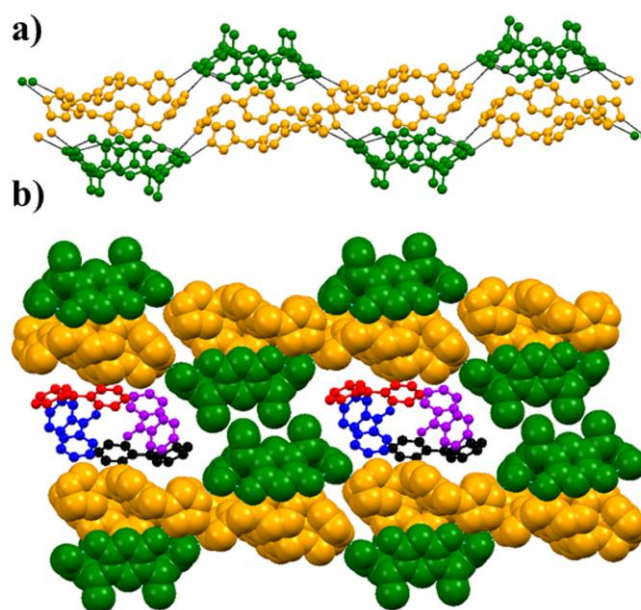


Fig. 2: Crystal structure illustration of bix-CMCR host...benzil inclusion compound. a) Double buckled hydrogen bonded chain sustained by O-H...N interaction (bix – orange; CMCR – green); b) parallel packing of the double buckled chains (shown in orange and green color with space-filled model), displaying the inclusion of benzil molecules (four benzil molecules are shown in distinct colors) within the channels created by the host.

The ability to form polymeric networks and secondary interactions (*vide supra*) make bis-imidazole ligands very attractive to be used in supramolecular chemistry. Owing to their intriguing structural diversity range from 1-D chains to 2-D layers and 3-D frameworks and their intrinsic porosity, this ligand shows a great potential to construct a wide range of coordination polymers (CPs)¹¹ with diverse applications such as sensing,^{12a} catalysis,^{12b} magnetism,^{12c} non-linear optics (NLO),^{12d} biosensing,^{12e} medical diagnostics,^{12f} energy storage and batteries,^{12g} data storage,^{12h} separation,¹²ⁱ biomedicine,^{12j} or to generate supramolecular hydrogels.^{12k} To date, different combinations of ligands (linker) and metal ions (node) have been explored for the synthesis of functional CPs. Although most of the ligands used are nitrogen donor pyridyl ligands¹³ less sterically hard imidazole ligands remained poorly explored until 2000,¹⁴ despite the well-established coordination chemistry of imidazole derivatives.¹⁵ In this perspective review, we focused on **bix**, the most popular bis-imidazole ligand. We have summarized the most interesting infinite structures of CPs derived from this ligand, not only based on the different coordination modes and structural chemistry but also based on their physicochemical properties and applications. The **bix** ligand typically binds metal ions through the N-donor imidazole group and its high degree of conformational flexibility in the ligand backbone lead to metal-ligand self-assembled CPs. The rotation of the C(sp³)–N(sp³) bonds causes different conformations namely *trans* or *gauche* (Scheme 1) that can affect the coordination geometry and the final polymeric structure. These properties make this ligand suitable to act as a building block for obtaining a wide number of CPs with interesting architectures and physicochemical properties. A Cambridge Structural Database¹⁶ (CSD version 5.36)¹⁷ search using Conquest v. 1.15¹⁸ resulted in 606 hits of CPs involving **bix** as ligand (ESI†). This review is not a comprehensive account of these 606 crystal structures. In fact, in keeping with the soul of a perspective review, it is a discussion of the intriguing topology of the ligand **bix** exhibited in some of the selected structures and its properties. Moreover, the review is rather a journey from crystalline to amorphous CPs as function of connectivity and degree of ordering based on **bix** characteristics. We will emphasize more in the material chemistry point of view, from the CPs as ordered supramolecular materials (crystalline) to more dis-ordered supramolecular assemblies (amorphous) and their attractive properties.

2. Crystalline CPs

CPs are generally highly crystalline materials thereby facilitating single crystal X-ray diffraction (SXRD) to elucidate their structures with atomic resolution that provide invaluable insights for developing design strategies and also analyse the structure-property correlation. Due to the tremendous number of crystal structures of CPs reported over the last 30 years using **bix** as ligand, for better understanding of readers, we discuss some of the most relevant examples restricting to those including as metal nodes Ag(I), Zn(II), Cd(II), Co(II), Cu(II), Fe(II) and Mn(II).

2.1. Ag-**bix** CPs

One of the first examples of crystalline structures of CPs containing **bix** was a silver-based polymeric material namely [$\text{Ag}_2(\text{bix})_3 \cdot (\text{NO}_3)_2$]_∞ (**1**) (crystallized in monoclinic *P2₁/n* space group),¹⁹ reported by R. Robson *et al.*, one of the pioneers of CPs synthesis and characterization. In the crystal structure of **1**, the metal ion Ag(I) exhibits trigonal planar geometry. Among the three crystallographically independent ligands of **bix**, two of them showed *gauche* conformation and the remaining one exhibit *trans* conformation. The *gauche* conformational ligands (angular

ligating topology) form a ($\text{bix}_2\text{-Ag}_2$) macrocycle (ring) via coordination of **bix** ligand with silver ions. Interestingly the linear conformation (rod) of the third **bix** ligand undergoes extended coordination with the macrocycles, resulted in the formation of a 1D-CP (Fig. 3). Such 1D coordination polymeric chains are further entangled each other via inclined fashion to generate a polyrotaxane structure sustained by $\text{C-H}\cdots\pi$ interaction involving the imidazole rings and aromatic phenyl ring.

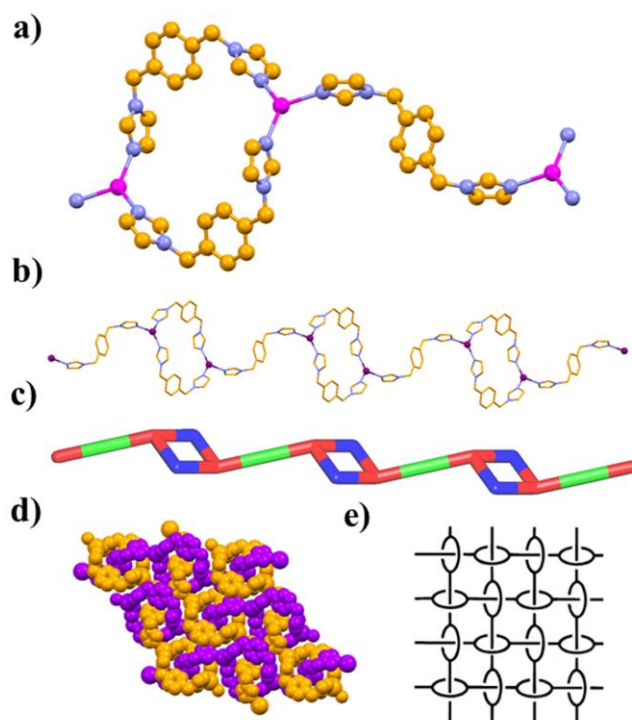


Fig. 3: Crystal structure illustration of **1** - a) The monomer unit of **1**, displaying the trigonal planar geometry of Ag(II) and different conformations of **bix**; b) 1D CP of **1** showing the ring and rod ligating topology of **bix**; c) TOPOS²⁰ view of 1D CP with color code: Ag – red, **Bix** – blue (*gauche*) and green (*trans*); d) 2D sheets of CP with polyrotaxane structure, 1D CPs are shown in orange and purple color; e) a schematic representation of polyrotaxane CP. Figure e) is reprinted from ref. 19 with permission. Copyright 1997, American Chemical Society.

The counter-anion nitrate was located within the interstitial space of the 2D sheets of CP involving hydrogen bonding with the imidazole functionality via $\text{C-H}\cdots\text{O}$ interaction. It is worthwhile to mention here that a polymorph of **1** was reported in 2005 namely $[\{\text{Ag}_2(\text{bix})_2\} \cdot (\text{NO}_3)_2 \cdot 2\text{H}_2\text{O}]_\infty$ (**1a**)²¹ crystallized in a low symmetric crystal system (triclinic P-1). In contrast to **1**, the metal ion Ag(I) in **1a** exhibit a linear geometry. The metal-ligand self-assembly resulted in a 1D wavy CP. The reason behind such coordination architecture is the linear coordination geometry of Ag(I) and “Z” shaped (*trans*) ligating topology of **bix** ligand. The parallel packing of such 1D wavy CPs resulted in nanopores. Interestingly the crystal structure exhibit another crystallographically independent Ag-**bix** polymeric chains passing through these nanopores supported by the $\pi\cdots\pi$ stacking interaction involving the phenyl rings of **bix** ligands. Such orthogonal packing of Ag-**bix** polymers lead to voids which are occupied by the nitrate counter-anion and lattice included water molecules (Fig. 4).

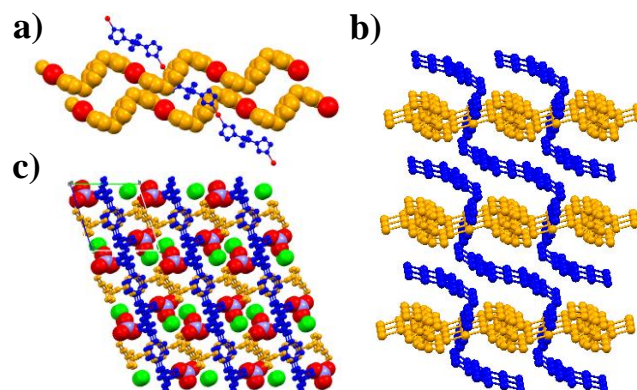


Fig. 4: a) Parallel packing of 1D CP **1a** (shown in orange-red – space-filled model), displaying nanopore and the crystallographically independent Ag-**bix** 1D CP (shown in blue-red) passing through the pore; b) orthogonal packing of 1D polymeric chains (crystallographically independent Ag-**bix** 1D CP chains are shown in orange and blue); c) Overall packing of 1D CP chains showing the occlusion of nitrate and water molecules (shown in pale blue-red and green color with space-fill model).

Later, Du *et al.* synthesized a Ag-**bix** CP namely $[\{Ag_4(CN)_4(bix)_2\}]_\infty$ (**2**)²² by replacing the anion NO_3^- with bidentate linear shaped anion CN^- . The asymmetric unit of **2** contains four crystallographically independent Ag atoms, four CN^- groups and two **bix** ligands. In the crystal structure, the metal ion exhibit slightly distorted trigonal planar geometry and the **bix** ligand showed less energetically favourable *gauche* conformation. The metal-ligand self-assembly leads to the formation of a *zigzag* polymer chain, which is the primary supramolecular architecture. Such chains are connected the 10-membered rings through two **bix** ligands, and finally generate a undulating 2D framework with cavities ($\sim 16 \cdot 13$ Å) along the crystallographic axis “a”. The cavities, however, are filled by another 2D framework of **2** and thus generate an interpenetrating double-layer structure which further stacked into a 3D supramolecular structure through π - π stacking involving imidazole rings of adjacent layers (Fig. 5). Interestingly, **2** showed strong photoluminescence properties at room temperature. Hong *et al.*, reported a 2D CP namely $[\{Ag_4I_4(bix)\}]_\infty$ (**3**)²³ by reacting **bix** with AgI. The crystal structure analysis of **3** revealed that the ligand adopted a linear ligating topology (*trans* conformation) and the metal- ligand polymerization generate a wavy like 2D network sandwiching Ag-I chains. Interestingly the 2D layers did not show any interpenetration, instead parallel packed on top of each other in {ABAB...} fashion supported by van der Waals force, and display 1D rectangular channels along “a” axis (Fig. 6). The CP **3** exhibits multiple emission properties (florescence and phosphorescence) in solid state when excited at 380 nm at room temperature and 10K.

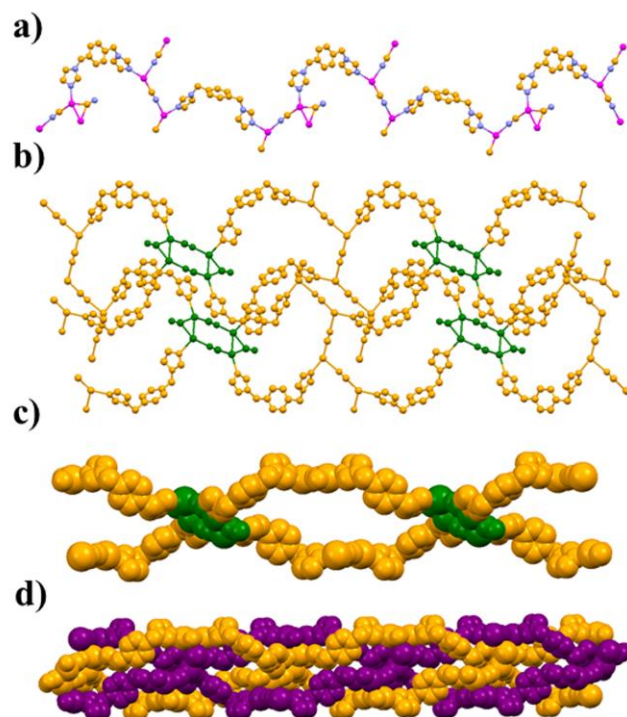


Fig. 5: a) 1D *zigzag* coordination polymeric chain in **2**; b) coordination driven self-assembly of 1D *zigzag* chain to 2D CP sheet, connected through the 10 membered ring (shown in green) in **2**; c) 2D CP sheet along 'a' axis displaying the cavity; d) two fold interpenetrated 2D CP (each sheets are shown in orange and purple color) in **2**.

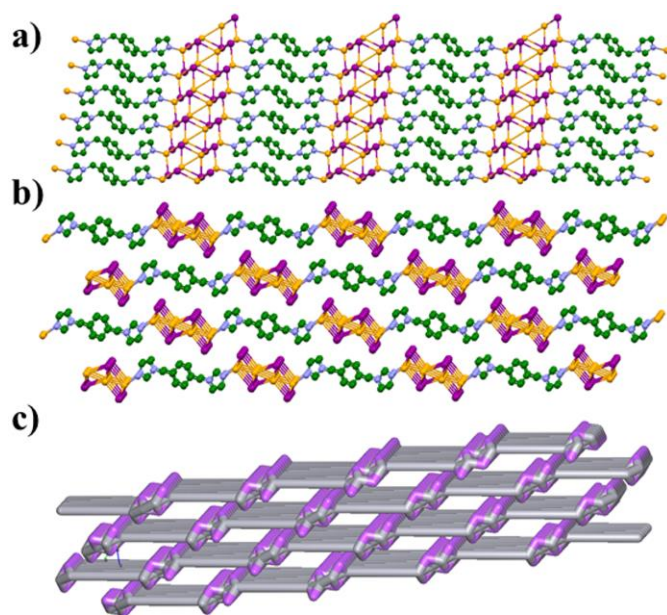


Fig. 6: a) 2D CP sheets of **3** generated from the self-assembly of Ag-I chains and **bix** having a *trans* conformation; b) {ABAB...} parallel packing of 2D CP displaying 1D rectangular channels along 'a' axis; c) TOPOS view of packing of 2D CP along 'a' axis.

2.2. Zn-bix CPs

First Zn-**bix** CP namely $[\{Zn(bix)_2\}(NO_3)_2 \cdot 4.5H_2O]_\infty$ (**4**)²⁴ was reported by Robson *et al.* in 1997. This structure also exhibits a 2D polyrotaxane structure like Ag-**bix**-NO₃ CP **1** with a completely different topology. The metal node Zn(II) showed a distorted tetrahedral coordination geometry in which all four coordination positions are bound by **bix**. In the crystal structure, two crystallographically independent ligands **bix** exhibit different conformation – *trans* and *gauche*. The Zn(II) coordination of ligand **bix** with *gauche* conformation resulted in the formation of a metallomacrocycle, and the extended coordination of **bix** ligands having *trans* ligating topology, lead to the generation of 2D polymeric sheet having microporous structure (Fig. 7). Unfortunately, the micro-pores are filled with another 2D polymeric sheet via interpenetration, preventing **4** for its using in sorption applications. In fact among the four fold coordination sites of Zn(II), two are coordinated with the *gauche* conformation of **bix** and the remaining two coordinated to the *trans* isomer resulting in alternate ring and rod topology. Thus there are three types of bridging **bix** ligands present in **4**, those that form the macrocyclic Zn(bix) rings, the rods that pass through these rings, and those that connect columns as showed in Fig. 7c-f. Water molecules and nitrate ions are present within the interstitial space of the 2D CP structure.

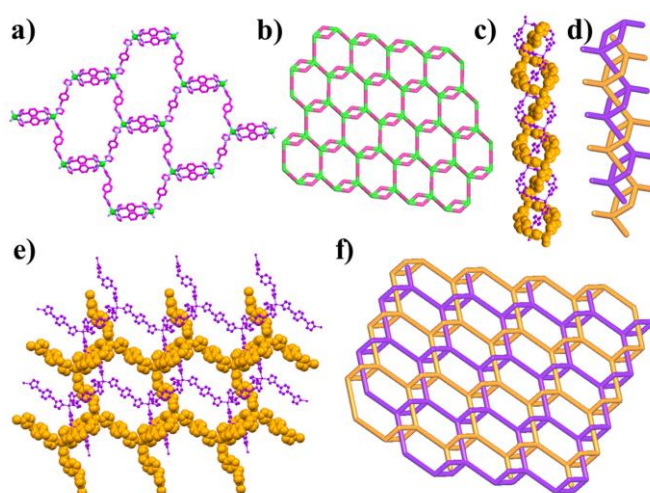


Fig. 7: a) 2D CP **4** with ring and rod ligating topology of **bix**; b) TOPOS²⁰ view of 2D CP; c)-f) two fold interpenetration of CP **4** displaying the polyrotaxane structure, (adjacent 2D CPs are shown in orange and purple color).

Later a topological isomer of CP **4**, namely $[\{(Zn)_2(bix)_4\} \cdot (NO_3)_4 \cdot 5H_2O]_\infty$ (**4a**) was reported by Chawla *et al.*²⁵ The Zn(II) ions exhibit distorted tetrahedral coordination geometry similar to **4**, and in both crystalline structures **bix** ligands coordinated to Zn alternatively in *gauche* and *trans* conformations. Unlike in **4**, no macrocycles (*ring*) were formed in the structure of **4a**. Although the coordination geometry of Zn(II) is close to tetrahedral the angular nature of **bix** acts as a pseudosquare planar node in the crystal structure of **4a**. The alternate *gauche* and *trans* conformation of **bix** ligands resulted in the formation of rectangular shaped 2D grid structure with corrugated sheet (wave like) architecture, which propagates in the 'ac' plane (Fig. 8a-b); the longer and shorter sides of the rectangle are generated from the *trans* and *gauche* conformation of **bix** ligands, respectively. The two nearest rhombic rows are arranged in such a way that the mirror images of each other and the centre of inversion passes through the centre of rectangular block. The 2D sheets are packed on top of each other resulted in a 3D entangled structure which enclose the channels

perpendicular to the plane of rectangular grid with a cavity size of $10 \times 5.5 \text{ \AA}$ (Fig. 8c). A view through the crystallographic axis 'a' revealed that such a parallel interpenetration did not affect the rectangular cavity (Fig. 8d-e). The counter-anions and lattice included water molecules are located in the rectangular channels and are highly involved in various hydrogen bonding and other non-bonded interactions.

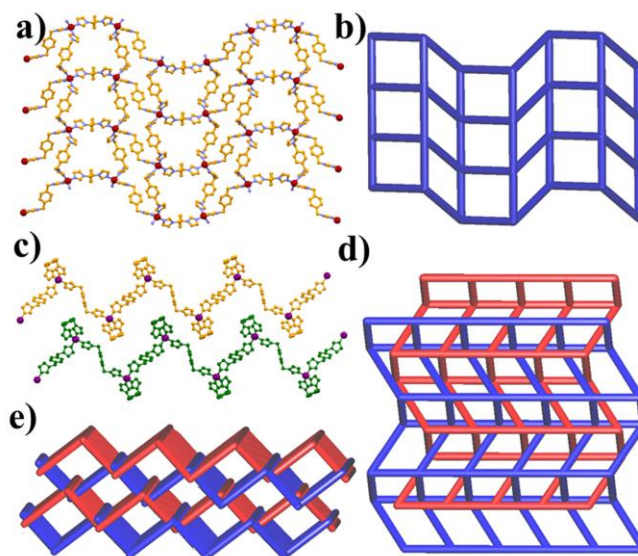


Fig. 8: a) Crystal structure and b) TOPOS view of rectangular shaped 2D grid structure with corrugated sheet (wave like) architecture in CP **4a**; c) parallel packing of 2D grids (adjacent grids are shown in orange and green, Zn(II) shown in purple); d)-e) parallel interpenetration of the 2D grids (adjacent grids are shown in blue and red color).

Carlucci *et al.*, reported a Zn(II) CP namely $[\{Zn_2(bix)_3(SO_4)_2\} \cdot 8H_2O]_\infty$ (**5**) having SO_4^{2-} as counter-anion.²⁶ Reaction of **bix** with $ZnSO_4$ in 1 : 2 metal-to-ligand ratio in H_2O -acetone resulted in single crystals of **5**. In the crystal structure, Zn(II) metal node exhibits distorted tetrahedral coordination geometry and are coordinated by three molecules of **bix** and one SO_4^{2-} . All the **bix** ligands adopted *gauche* conformation; two of them form macrocycles with Zn(II) metal nodes and the third ligand extended the coordination resulted in an infinite 1D CP with alternate rings and rods like architecture. The polymeric chains are highly undulated and propagate in [1 0 1] direction and are interlocked with two adjacent chains resulted in the formation of a 2D polyrotaxane layer. The X-ray structure of **5** also reveals that C-H $\cdots\pi$ interactions involving the phenyl and imidazole rings play a crucial role in stabilizing such entangled 1D \rightarrow 2D arrays. In fact the topology of networks interlocking in **5** is parallel fashion in contrast to the inclined style in **1** (Fig. 9). The 2D sheets are packed on top of each other and the voids present between these sheets were occluded with lattice included water molecules; upon heating until 100°C, the occluded water molecules were removed but retain its crystallinity and framework integrity, although reversible sorption of water molecules resulted in change of crystalline phase of **5** as revealed from powder X-ray diffraction (PXRD).

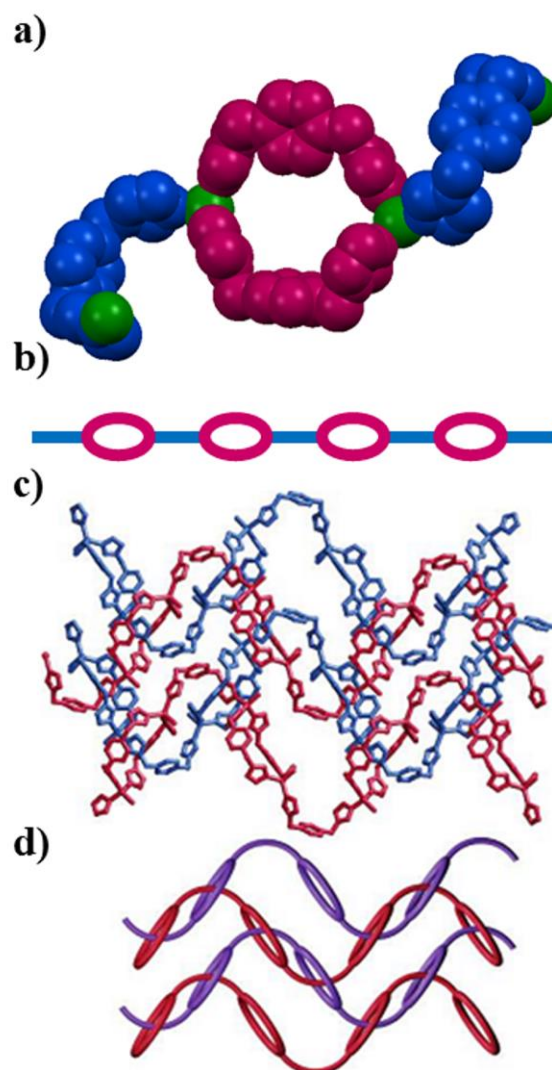


Fig. 9: Crystal structure illustration of **5**; a) metallo-macrocycle or ring (purple color) and rod topology (blue) of **bix** in **5**; b) schematic representation of 1D CP formed by **bix** with ring and rod ligating topology; c) parallel interlocking of 1D undulated chains in the polyrotaxane; d) schematic view of the interpenetration. Fig. 6c and 6d are reprinted from ref. 26 with permission. Copyright 2005, American Chemical Society.

Recently a Zn(II) coordination complex (CC) namely $[\{Zn_2(bix)_2(Br)_2\}]$ (**6**)²⁷ with bromide as counter-anion was reported. The *gauche* conformation of the ligand and distorted tetrahedral geometry of Zn(II) (each two coordination sites were occupied by Br and **bix**) resulted in a 26 membered ring metallo-macrocycle. In this non-polymeric material, interestingly the metallo-macrocycle packed into a 3D hydrogen bonded porous network sustained by C-H \cdots Br interaction involving the imidazole moiety and metal bound bromide anion.²⁷ Although well-defined nanosize pores were observed in this architecture, no sorption properties of **6** was reported. Curiously, when ZnCl₂ is used as metallic salt in the synthesis, the resulting material show a 1D CP $[\{Zn(bix)(Cl)_2\}]_\infty$ (**7**).²⁸ In this case, the **bix** ligand exhibited *trans* conformation, and the metal ion Zn(II) showed a distorted tetrahedral geometry with two coordination positions occupied by **bix** and the other two by chloride. The *trans* conformation of the ligand and its infinite coordination with the Zn(II) node resulted in a 1D *zigzag* CP. The adjacent polymeric chains are interact each other

via C-H...Cl hydrogen bonding involving the phenyl and imidazole ring with the metal bound Cl atom, and such interaction resulted in the formation of a 2D hydrogen bonded sheet. Interestingly, such sheets are further packed on top of each other in an orthogonal fashion via various hydrogen bonding and other weak interactions (Fig. 10).

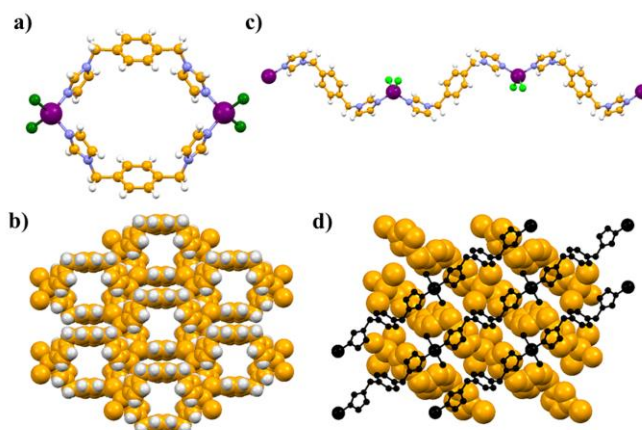


Fig. 10: a) metallo-macrocycle **6** displaying gauche conformation of **bix**; b) self-assembly of metallo-macrocycle **6** displaying microporous hydrogen bonded network; c) 1D zigzag CP **7**; d) orthogonal packing of 1D chains of CP **7** (adjacent 2D hydrogen bonded sheets are shown in orange and black color).

The evident influence of the counter-anion in these systems become apparent in another Zn(II)-**bix** CP reported by Hanson *et al.* In this case, hydrothermal reaction of $\text{Zn}(\text{OAc})_2 \cdot 2\text{H}_2\text{O}$ and **bix** in presence of KH_2PO_4 resulted in the crystallization of a 2D CP namely $[\{\text{Zn}_2(\text{HPO}_4)_2(\text{bix})\} \cdot 2\text{H}_2\text{O}]_\infty$ (**8**).²⁹ SXR analysis of **8** revealed that the **bix** ligand adopts *trans* conformation, while the Zn(II) exhibit tetrahedral geometry with three coordination sites occupied by O atoms of three different HPO_4^{2-} anions and the remaining one by **bix**. In fact in **8**, ZnO_3N and HPO_4^{2-} groups are connected to form an edge-shared inorganic ladder structure composed of four rings. The inorganic ladders within a layer are parallel and linked together by **bix** to form the 2D CP structure (Fig. 11a). The 2D layers are further connected by hydrogen bonding to form the 3D structure in an AAA arrangement. The lattice included water molecules are occluded within the interstitial space of 2D layers sustained by hydrogen bonding. Later the same group reported a 3D Zn(II)-phosphite CP namely $[\text{Zn}(\text{HPO}_3)(\text{bix})_{0.5}]_\infty$ (**9**).³⁰ They described the structural transformation of 2D in **8** to 3D in **9** due to the reaction conditions. In contrast to the hydrothermal reaction used for the synthesis of **8** (reaction of $\text{Zn}(\text{OAc})_2 \cdot 2\text{H}_2\text{O}$, KH_2PO_4 , **bix** in water for 9 days at 130°C), $\text{Zn}(\text{OAc})_2 \cdot 2\text{H}_2\text{O}$, H_3PO_3 , NaOH and **bix** were hydrothermally reacted at 125°C for 10 days and yielded block shaped crystals of **9**. In the crystal structure of **9**, the Zn(II) are tetrahedrally coordinated by three O atoms and one N atom of **bix**. It is interesting to note that the ZnO_3N and HPO_3 groups are coordinated to form a polymeric inorganic 2D network displays 4.8^2 topology (Fig. 11b). In fact this 2D layer structures was interconnected by pillar **bix** ligands which coordinate to Zn(II) via Zn-N_{bix} coordination with the consequent formation of the 3D CP (Fig. 11c). The two imidazole groups of the **bix** ligand extend to both sides of the benzene ring, with a dihedral angle between the benzene ring and the imidazole plane of 74.3° . Thus, the **bix** ligand exhibits a *trans* conformation which induces highest dimensionality (3D) in **9**.

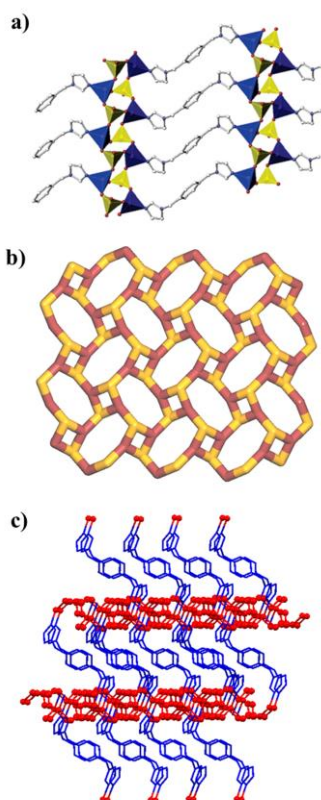


Fig. 11: a) 2D coordination polymeric sheet of **8**, displaying the inorganic ladders of ZnO_3N (blue) and HPO_4 groups (yellow); b) 2D infinite sheet of Zn(II)-HPO_3 units, displaying 4.8^2 topology; c) 3D CP **9** obtained from the pillaring of **bix** (blue) through the 2D infinite sheet 4.8^2 (shown in red color in ball and stick model) of Zn(II)-HPO_3 units. Fig. 11a is reprinted from ref. 29 with permission. Copyright 2005, American Chemical Society.

2.3. Cd-bix CPs

Cd(II) CPs derived from **bix** with different anions such as ClO_4^- , NO_3^- , SO_4^{2-} , Cl^- and SCN^- were reported by various research groups. Robson *et al.* reacted **bix** with $\text{Cd}(\text{ClO}_4)_2$ and $\text{Cd}(\text{NO}_3)_2$ separately, which resulted in 3D CPs namely $[\{\text{Cd}(\text{bix})_3\} \cdot (\text{ClO}_4)_2 \cdot 0.7\text{MeOH}]_\infty$ (**10**) and $[\{\text{Cd}(\text{bix})_3\} \cdot (\text{NO}_3)_2]_\infty$ (**11**),³¹ respectively. The authors deliberately designed and synthesize these 3D CPs, aiming for getting an α -polonium like coordination network. In the crystal structure of α -polonium crystal, each polonium atom is bound to six equivalent ones at the vertices of an octahedron, giving rise to a simple cubic network. Such network topology is possible only for octahedral metal ions (nodes) surrounded by six organic ligands (linkers). The most successful ligand 4,4'-bipyridine is not suitable candidate for the construction of α -polonium nets, due to the steric hindrance between ortho-hydrogen atoms which make it difficult to coordinate to six different pyridyl ligands around an octahedral metal ion. Such collisions between the ortho-hydrogen atoms can be avoid if we use five membered N-heterocycles, such as bis-imidazole ligand **bix**, and deliberately achieve MN_6 (M = metal ion, N = N donor ligand) octahedral coordination geometry (O_h). In order to avoid the competition of other ligands (i.e. solvent molecules or anions) for the coordination sites, the metal salt was reacted with **bix** in 1 : 3 molar ratio, the metal salt was dissolved in methanol solution and triethyl orthoformate was employed as a dehydrating agent.

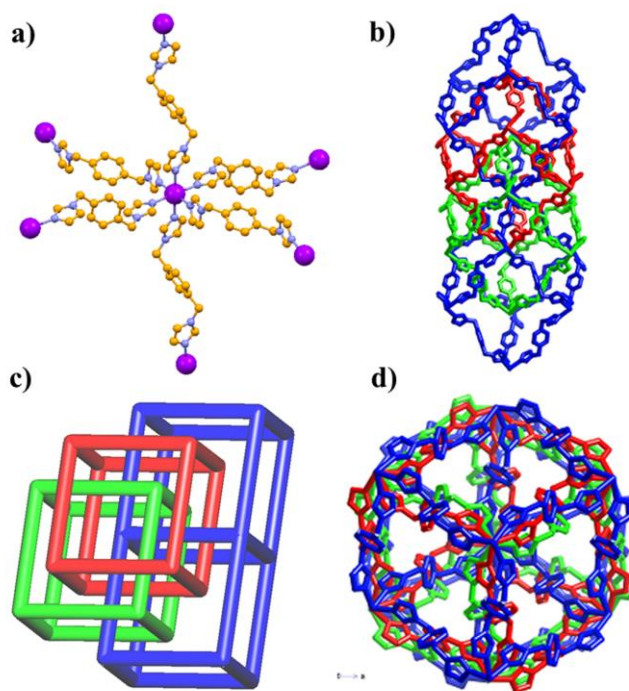


Fig. 12: a) octahedral coordination geometry and Cd(II) and the hexa coordinated **bix** in **10** (color code: Cd – purple, C – orange, N – pale blue); b) 3-fold interpenetration in **10** (adjacent networks are shown in blue, red and green color); c) TOPOS²⁰ view of interpenetration; d) view of interpenetration down to 'c' axis displaying the triangular shaped channels in **10**. Fig. 11b-11d are reprinted from ref. 31 with permission. Copyright 2002, Royal Society of Chemistry.

In the resulting crystal structures, **10** (trigonal R-1) and **11** (triclinic P-1), the ligand **bix** adopted a linear *trans* conformation. In both structures the octahedral coordination environment of Cd is occupied by six **bix** ligands (Fig. 12a). The extended coordination of **bix** with Cd resulted in a 3D CP having α -polonium topology and such networks are then interlocked with the adjacent networks lead to 3-fold interpenetration. In fact out of the three interpenetrated networks, one is crystallographically independent (blue net in Fig. 12b 12c) and the remaining two are related to each other by a center of inversion (red and green in Fig. 12b and 12c). The interpenetrated networks interplay each other via various intermolecular interactions involving the counter-anion perchlorate. Moreover, even after three fold interpenetration channels of approximately triangular cross-section [Fig. 12d] were present in the crystal structure and are occupied by two crystallographically unique perchlorate ions. In the crystal structure of **11** three crystallographically equivalent interpenetrating α -polonium-like networks were observed and the nitrate anions are located within the generated triangular shaped channels. When the competition between **bix** and other ligands (solvent, counter-anions) is not avoided during the synthesis, the resulting structure ends up with a 1D or 2D CPs. For example, a 1D CP namely $[\text{Cd}(\text{bix})(\text{NO}_3)_2(\text{DMF})_2]_\infty$ (**12**)³² (where DMF = *N,N*-Dimethylformamide) was reported by Prabusankar *et al.* by reacting $\text{Cd}(\text{NO}_3)_2$ with **bix** in 2 : 1 molar ratio in a DMF/chloroacetic acid under hydrothermal conditions. The resulting structure of **12** reflects a Cd(II) distorted octahedral geometry, where the six coordination sites are occupied by two **bix** ligands in *trans* conformation, two DMF molecules and two nitrate ions arranged in opposite positions (Fig. 13a). The coordination polymerization of **bix** along the 'c' axis resulted in a 1D *zigzag* CP.

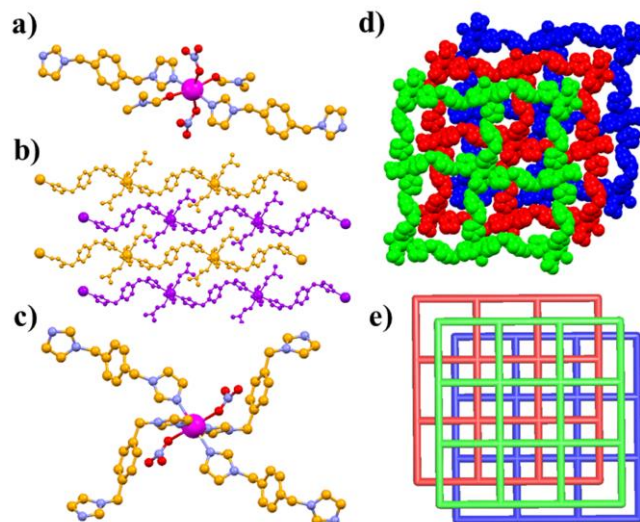


Fig. 13: a) Coordination geometry of Cd(II) in **12**; b) 1D *zigzag* CP chains of **12**; c) Coordination geometry of Cd(II) in **13**; d) the off-set packing of (4,4) grids in **13**; e) TOPOS²⁰ view of off-set packed (4,4) CP grids in **13**.

Such *zigzag* CP chains are packed in a parallel fashion along 'c' axis supported by C-H $\cdots\pi$ interaction involving CH₂ spacer of **bix** and π electron cloud of imidazole moiety, and C-H \cdots O hydrogen bonding of phenyl ring (C-H) with the O atom of metal bound nitrate anion resulting in a 2D hydrogen bonded sheet (Fig. 13b). The same reaction performed by reacting **bix** with Cd(NO₃)₂ (2:1 ratio) in a methanolic solution at room temperature resulted in a 2D CP namely [Cd(bix)₂(NO₃)₂]_∞ (**13**).³³ The SXRD analysis of the obtained colourless single crystals revealed a distorted octahedral geometry for Cd(II) in which axial positions are occupied by **bix** ligands in *trans* conformation, and the equatorial positions with the nitrate anions (Fig. 13c). The extended coordination of the **bix** ligand with the Cd(II) nodes resulted in a 2D CP with (4,4) grid like architecture. Such (4,4) grids are packed on top of each other in an off-set fashion and such packing effectively blocked the micropores (Fig. 13d-e). The interactions behind this packing correspond to weak C-H \cdots O hydrogen bonding involving the C-H of phenyl ring and imidazole moiety of **bix** with the O atoms of coordinated nitrate anion.

As observed from previous examples, the use of different counter-anions induce changes in coordination sphere and consequently on CPs supramolecular architecture. Thus, Carlucci *et al.* reported two different CPs namely [Cd₂(bix)₃(SO₄)₂]_∞ (**14**) and [Cd₂(bix)₂(H₂O)₄(SO₄)₂·bix]_∞ (**15**) obtained from the reaction of CdSO₄ with **bix** in 1 : 2 metal-to-ligand ratio by slow diffusion of ligand solution with metal salt solution at room temperature.²⁶ In fact, two different crystalline structures are formed concomitantly (65 vs. 35% respectively) during crystallization process. It is worthwhile to mention here that a fast precipitation of CP by reacting **bix** with CdSO₄ in a 1 : 1.5 molar ratio resulted exclusively in the kinetic product **15**. In fact **14** and **15** crystallized in same crystal system monoclinic, but different unit cell settings (*P*₂₁/*n* for **14** and *P*₂₁/*c* for **15**). The unit cell of **15** showed more big volume than **14** (**15** - 2340.02 Å³, **14** - 2209.41 Å³), which is required for the inclusion of free **bix** molecules as observed in the crystal lattice. In the crystal structure of **14**, the metal centers exhibits distorted trigonal bipyramidal geometry and are bound by three imidazole groups of **bix** and two bidentate sulfate anions. Among these three coordinated **bix** ligands, two showed *gauche* conformation interconnecting two metal ions in a metallo-macrocycle and the third **bix** ligand

showed *trans* conformation extending the coordination polymer. The resulting 1D CP chain alternate ring and rod shaped topology as primary supramolecular structure (Fig. 14a), close to that shown in **1** and **5** CPs (*vide supra*). Such 1D chains are connected each other via sulfate bridging with the consequent formation of a 2D network (Fig. 14b). Interestingly, **14** and **1** are isomorphous; the 2D layers are close similar, the only difference is that in the case of **14** the anion (sulfate) bridged the adjacent 1D chains, whereas in **1** the nitrate anion is present in the crystal lattice as a guest.

On the other hand, **bix** ligands in **15** adopt *trans* conformation in the crystal structure. The Cd(II) exhibit distorted octahedral geometry, its equatorial positions are occupied by two **bix** and two sulfate anion in opposite fashion and the axial positions are occupied by two water molecules. Sulfate anion acts as a bidentate bridge ligand between metal ions. The extended coordination polymerization resulted in 2D (4, 4) layers of rhombic meshes. The axial coordinated water molecules interact with the occluded (un-coordinated guest) **bix** ligand via N-H...O hydrogen bonding (Fig. 14c).

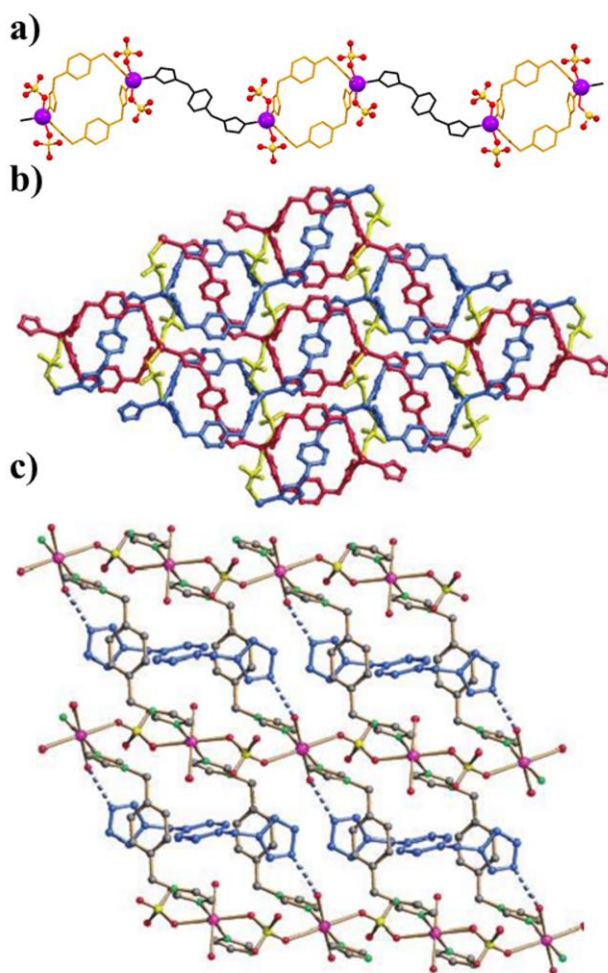


Fig. 14: a) 1D CP chain, the primary supramolecular architecture in **14**, displaying the *trans* (black color) and *gauche* (orange color) conformation of **bix**; b) 2D polyrotaxane CP **14** having inclined interlacing of the chains (adjacent chains are shown in red and blue color; sulfate is shown in yellow); c) 2D CP **15**, showing the hydrogen bonding of occluded **bix** ligand (blue) with coordinated water molecules. Fig. 13b-11d are reprinted from ref. 26 with permission. Copyright 2002, American Chemical Society.

It is sensible to mention that another polymorph of **14** and **15** namely $[\{\text{Cd}(\text{bix})_{0.5}(\text{H}_2\text{O})_2(\mu_3\text{-SO}_4)\} \cdot \text{H}_2\text{O}]_\infty$ (**16**) was reported by Liu *et al.*³⁴ This additional CP was synthesized by hydrothermal method by mixing 2 : 1 metal-to-ligand molar ratio and crystallized in the same space group of **15**, $P2_1/c$, but the unit cell volume of **16** (1240.07 Å³) is

notable inferior in comparison with **14** or **15**. The metal center exhibit distorted octahedral geometry in which the equatorial positions are coordinated by three sulfate anions and one water molecule, and the axial positions are occupied by **bix** and other water molecule (Fig. 15a). The sulfate anion acts as a tridentate ligand (μ_3) and its coordination polymerization with Cd(II) lead to the formation of a 2D inorganic CP having a binodal 4.8^2 topology (Fig. 15b-c).

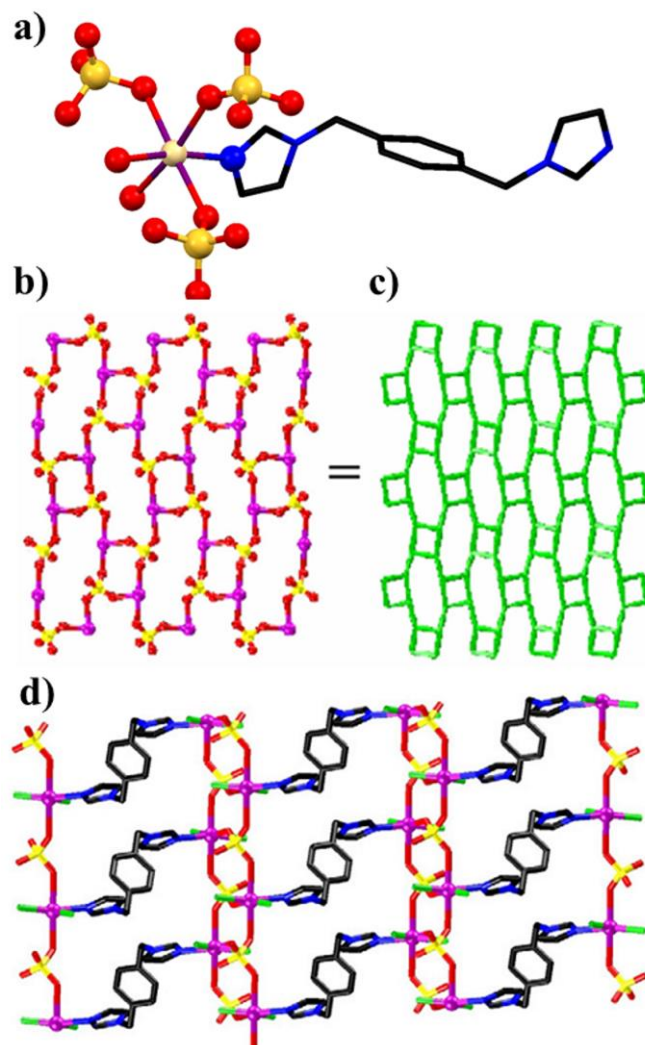


Fig. 15: a) Coordination geometry of Cd(II) in CP **16**; b) The 4.8^2 CdSO₄ inorganic 2D network c) TOPOS view of 2D inorganic network; d) 3D coordination polymer in CP **16**. Fig. 14b-d are reprinted from ref. 34 with permission. Copyright 2007, Elsevier B.V.

The coordination driven self-assembly of *trans* conformation of **bix** ligand through the Cd(II) node of 2D CdSO₄ inorganic sheet, resulted in a 3D open framework structure, whose cavities are occupied with solvated water molecules (Fig. 15d). Interestingly, this CP shows room temperature photoluminescence properties.

Recently, Dan *et al.* reported a 3D Cd(II) CP namely $[\{Cd_2(bix)_4(SCN)_4\}]_\infty$ synthesized by hydrothermal reaction of Cd(OAc)₂·2H₂O, **bix** and NaSCN in a 1:1:1 molar ratio. (**17**).³⁵ The resulting CP showed an asymmetric unit that contains four crystallographically unique Cd(II)-atoms, four **bix** ligands and four SCN⁻ anions. Three Cd(II) centers show octahedral coordination geometry {CdN₆}, which is completed with four N-atoms from four **bix** ligands, and two N-atoms from two SCN⁻ anions. The forth Cd(II) cation is coordinated to four **bix** ligands via N-atoms and two

SCN⁻ anions via S-atoms. The four **bix** ligands adopting both an overall *gauche* configuration but different conformational parameters such as N–C_{sp3}···C_{sp3}–N and N_{donor}···N–C_{sp3}···C_{sp3} torsion angles, as well as M···M and N_{donor}···N_{donor} distances. In this way, eight Cd(II)-ions are linked through four pairs **bix** bridges to form a rare centrosymmetric, 104-membered ring of [Cd(**bix**)]₈ (Fig. 16a). The coordination polymerization of such ring resulted in a 3D framework of 4².8⁴-1vt net having a pore size as large as zeolites (Fig. 16b). Unfortunately the pores are blocked by another two distinct 3D networks via 3-fold interpenetration (Fig. 16c and 16d).

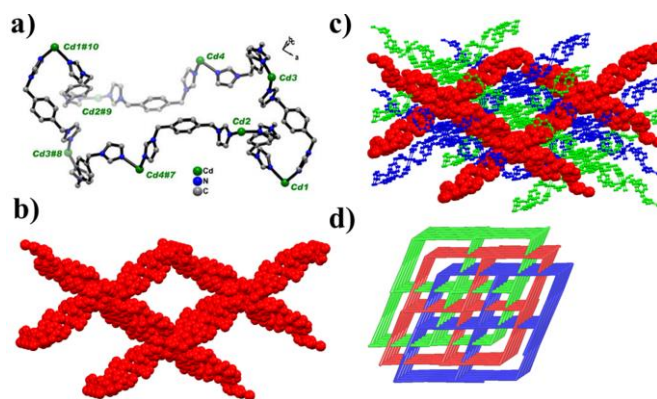


Fig. 16: a) A single 104-membered ring [Cd(**bix**)]₈ in **17**; b) 3D porous framework of CP **17**; c) and d) are the crystal structure and TOPOS representation of 3-fold interpenetration in CP **17**, respectively (independent networks are shown in red, blue and green color). Fig. 16a are reprinted from ref. 35 with permission. Copyright 2013, Springer.

2.4. Co-**bix** CPs

Octahedral/tetrahedral Co(II)-**bix** nodes were also explored by various research groups in the designing and synthesis of CPs. Carlucci et al self-assembled a CP namely [$\{Co(bix)_2(H_2O)_2\} \cdot (SO_4) \cdot 7H_2O\}_\infty$ (**18**) by reacting CoSO₄ and **bix** in 1 : 2 metal-to-ligand ratio by slow diffusion method.³⁶ In the crystal structure, two different metal-organic motifs (crystallographically independent) are present; both of them exhibit octahedral geometry for Co(II) in which the equatorial position are occupied by **bix** ligands and the axial positions by water molecules. The only difference is the conformation of **bix** ligand. Thus, one of the motifs is related to the extended coordination of the *gauche* conformed **bix** affording a 1D looped chain CP which runs parallel to the [010] direction (Fig. 17a). On the second motif, the *trans* conformation of **bix** lead to the formation of a 3D network of four-connected nodes with the (6⁵.8) CdSO₄ topology. In fact the 1D CP loop chains undergo (1D + 3D) to an entanglement with the 3D CP via catenation (Fig. 17b). Even after entanglement, **18** exhibits very large channels that are filled with counter-anion SO₄²⁻ and lattice included water molecules.

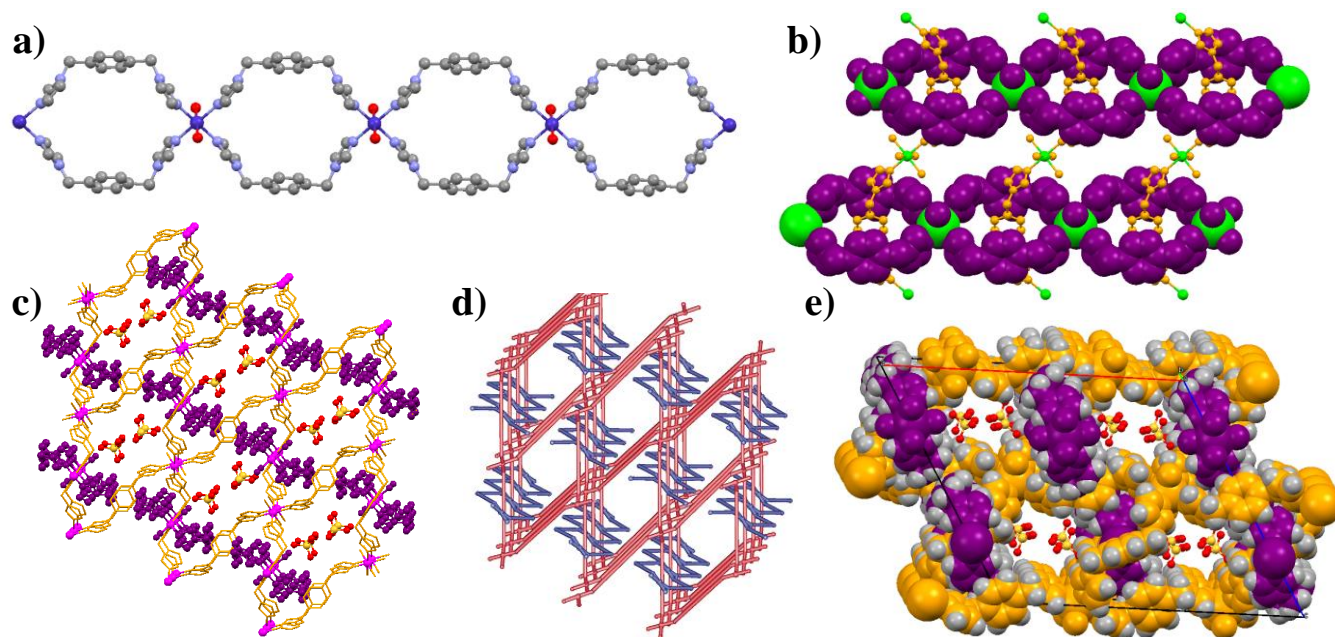


Fig. 17: a) 1D looped chain CP of motif 1 in CP **18**; b) the entanglement of 1D looped chain over the 3D framework in **18** (only a part of 3D framework is shown for clarity), displaying the gauche and trans conformation of **bix**; c) (1D + 3D) type entanglement in **18** (the 3D framework is shown in orange color and the 1D loop CP is shown in purple color); d) its TOPOS representation; e) the entangled network, displaying the channels and occluded sulfate counter-anion. Fig. 16d is reprinted from ref. 36 with permission. Copyright 2004, Royal Society of Chemistry.

The effect of solvent on the final structure of CP was elegantly demonstrated with this system. Thus, a polymorph of **18** namely $[\{\text{Co}(\text{bix})(\mu_2\text{-SO}_4)(\text{H}_2\text{O})_2\}]_\infty$ (**19**) was synthesised by reacting **bix** and CoSO_4 in 2 : 1 ligand-to-metal ratio by using $\text{MeOH}/\text{CHCl}_3$ or $\text{MeOH}/\text{acetone}$ solvent mixture (in the case of **18**, $\text{H}_2\text{O}/\text{Acetone}$ was the solvent).³⁶ The SXRD analysis revealed that the structure of **19** consisted of a Co(II) node exhibiting distorted octahedral geometry in which the equatorial positions are occupied by two sulfate and two **bix** ligands adopting *gauche* conformation, and the axial position are coordinated by two molecules of water (Fig. 18a). The polymerization of **bix** and sulfate (act as a bidentate ligand) with Co(II) node lead the formation of a 2D corrugated sheet CP. These highly undulated simple polymeric chains (with gauche conformation of the **bix** ligands) are connected by bridging sulfates into 2D (4,4) layers (Fig. 18b). The 2D sheets are packed exactly on top of each other along the b-axis stabilized by various weak interactions, which showed nano-porous structure (Fig. 18c-d). The formation of this polymorph is probably due to the fact that, in contrast to water, the solvents used are not efficient in preventing the coordination of the sulfate anions to the metal.

Another curious Co-**bix** coordination polymer was reported by Zhao and co-workers.³⁷ They reported the structure of the CP obtained by reaction of $\text{Co}(\text{CH}_3\text{COO})_2$ with **bix** and NaNO_2 in a methanol/water solution resulted in an open 3D framework namely $[\{\text{Co}(\text{bix})_3\} \cdot 2\text{OH} \cdot \text{CH}_3\text{OH} \cdot 3\text{H}_2\text{O}]_\infty$ (**20**). The crystal structure revealed an octahedral coordination for Co(II) with all the positions occupied **bix** ligands (Fig. 19a). The **bix** ligand adopted *trans* conformation, and its infinite coordination with Co(II) resulted in a 3D coordination polymer having open diamond-shaped cavities ($8.43 \times 8.43 \text{ \AA}$), which are filled guest OH^- , solvated methanol and water molecules (Fig. 19b). Magnetic susceptibility measurement revealed the presence of weak antiferromagnetic interactions in complex **20**.

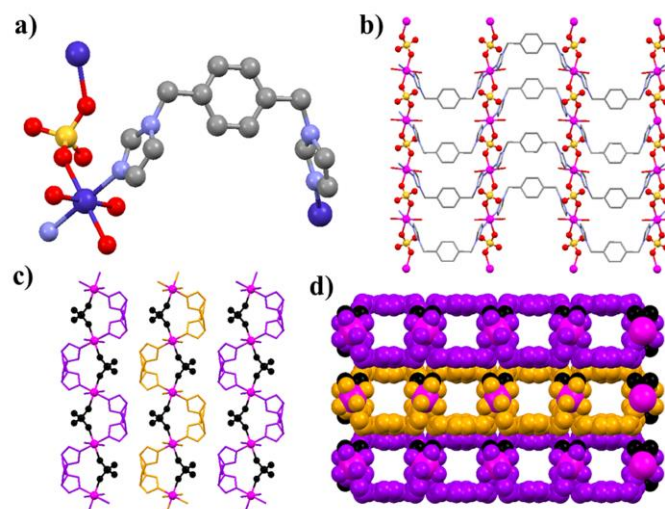


Fig. 18: a) Coordination environment of Co^{II} in **19**; b) 2D corrugated sheet architecture in **19** due to sulfate bridging and 1D polymerization of **bix** with gauche conformation (sulfate is shown in ball and stick model); c) parallel packing of 2D sheets in **19**; d) parallel packing of 2D sheets along 'b' axis, displaying the nano-pores in **19**.

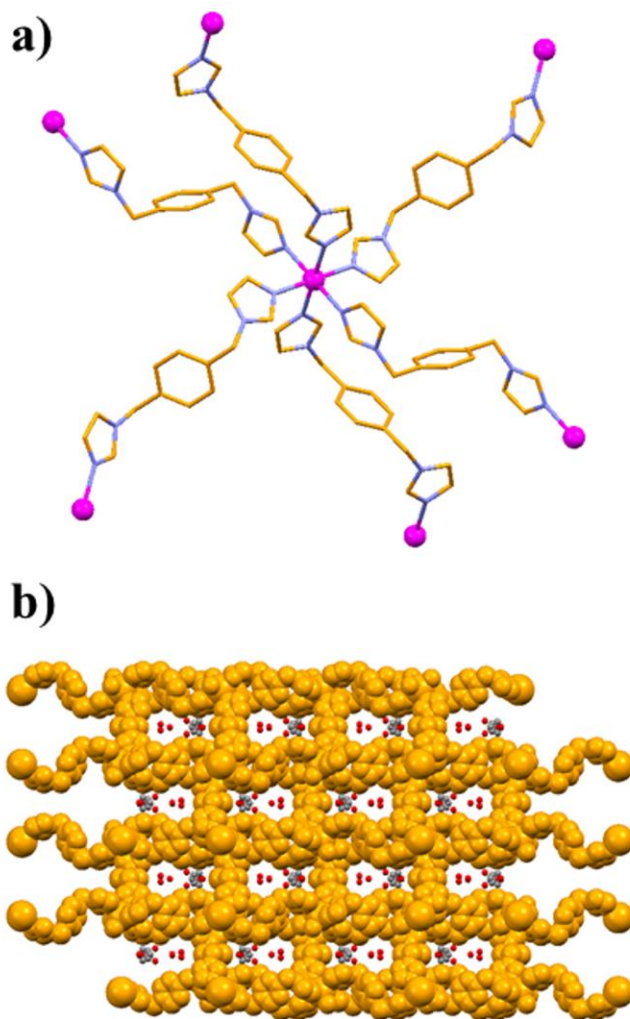


Fig. 19: a) Coordination environment of $\text{Co}(\text{II})$ in **20**; b) 3D 3D CP **20** (shown in orange) displaying the occlusion of OH^- and solvents (red and grey color in ball and stick model) within the infinite channel.

The occlusion of other anionic species with Co-**bix** CPs was reported by Hanson et al.³⁸ In this occasion phosphate anion was incorporated to a 2D CP namely $[\{\text{Co}(\text{bix})_{0.5}(\text{HPO}_3)\} \cdot 3\text{H}_2\text{O}]_\infty$ (**21**). In this polymeric material Co(II) showed a distorted tetrahedral coordination geometry in which three position are coordinated by HPO_3 anions and the last one by **bix** ligand. The **bix** ligand exhibits *trans* conformation, and the coordination of HPO_3 and Co(II) resulted in the formation of an inorganic cluster infinite 1D chain. Such chains are further bridged by **bix** ligand which leads to the generation of a 2D CP. The temperature-dependent magnetic susceptibility measurements of **21** showed weak interactions between the Co(II) centers.

2.5. Cu-**bix** CPs

One of the most successful metal node in CP chemistry, Cu(II), has been also explored by various research groups to synthesize **bix**-related CP. The numerous examples of Cu-**bix** polymeric networks reveal some important factors that determine the structure of the resulting material such as type of counter-anion or synthetic methodologies. Thus, the reaction of $\text{Cu}(\text{OAc})_2$ with **bix** in methanol resulted in a CP namely $[\text{Cu}_2(\text{ac})_4(\text{bix})_2]_\infty$ (**22**)³⁹ which showed two different (crystallographically independent) metal-organic motifs. Both have similar Cu(II) octahedral coordination environment in which the equatorial positions are coordinated by acetate (ac) anion (in a chelate fashion) and axial positions are coordinated by *trans* conformation **bix**. The coordination driven self-assembly of **bix** with Cu(II) resulted in a 1D *zigzag* CP chains (first motif). Such chains are packed in parallel fashion resulted in voids that are crossed by other 1D CP chains belong to second motif run through this voids with an angle of 45° (Fig. 20a). Such packing finally resulted in a 3D hydrogen bonded supramolecular structure, although the metal-ligand coordination is 1D.

A carbonate (CO_3^{2-}) anion derivative of Cu-**bix** CP namely $[\{\text{Cu}_2(\text{CO}_3)_2(\text{bix})_3\} \cdot (\text{bix}) \cdot 10\text{H}_2\text{O}]_\infty$ (**23**) was also reported.⁴⁰ The Cu(II) metal centre exhibits unusual highly distorted square-based pyramidal geometry, in which equatorial positions are coordinated by two **bix** ligand and the other two positions by the carbonate anion in a chelate fashion. The apical position is occupied by other **bix** ligand. The **bix** ligands exhibit *trans* and *strained-gauche* conformations in the crystal structure. The extended coordination (*strained-gauche*) and bridging of **bix** between Cu(II) centers resulted in an infinite 1D ladder structure. The 1D ladders are self-assembled via non-bonded interactions in an ABAB- stacking sequence. (Fig. 20b). Such packing resulted in interstitial space occupied by water and guest **bix** molecules. Using $\text{Cu}(\text{NO}_3)_2$ as metal salt the **bix** ligand coordinate the Cu(II) formed a 2D CP namely $[\{\text{Cu}(\text{NO}_3)_2(\text{bix})_2\} \cdot \text{H}_2\text{O}]_\infty$ (**24**).⁴¹ In the crystal structure, the Cu(II) exhibit octahedral geometry and the ligand show *trans* conformation. The equatorial positions of Cu(II) are occupied by **bix** and the axial positions by nitrate anions. The infinite coordination of **bix** lead to the formation of a 2D CP having a (4,4) square grid structure (Fig. 20c). Such 2D CPs packed in an ABAB fashion, in which A's and B's are interact each other by $\text{O}-\text{H} \cdots \text{O}$ hydrogen bonding involving the metal bound nitrate and lattice included water molecules and lead to the formation of a 3D hydrogen bonded structure. Two sulfate derivative Cu(II) CPs namely $[\{\text{Cu}(\text{bix})(\text{H}_2\text{O})_3(\text{SO}_4)\} \cdot \text{H}_2\text{O}]_\infty$ (**25**) and $[\{\text{Cu}(\text{bix})_2(\text{SO}_4)\} \cdot 7.5\text{H}_2\text{O}]_\infty$ (**26**) were reported by Carlucci et al.⁴² Both **25** and **26** were obtained from the reaction of CuSO_4 and **bix** in water-acetone solvent mixture in which the stoichiometric ratio of metal-to-ligand were 1 : 1 and 1 : 3, respectively. In the crystal structure of CP **25**, Cu(II) showed distorted octahedral coordination geometry and its equatorial positions (two each) are engaged with N atoms of **bix** and O atoms of water molecules in *cis* position, and axial positions are occupied by one sulfate anion (mono-dentate fashion) and one water molecule. The polymerization

of **bix** and Cu(II) lead to the formation of a 1D highly undulated CP chains. These chains are further self-assembled through hydrogen bonding involving the metal bound sulfate, coordinated water and lattice included water molecules. In fact such hydrogen bonding resulted in a $\text{H}_2\text{O}\cdots\text{SO}_4^{2-}$ hydrogen bonded columnar frames, which connects the 1D CP chains (Fig. 20d). On the other hand, the asymmetric unit of **26** contains two Cu(II), two **bix** ligands (*trans* and *gauche* conformations, each coordinated to two different Cu^{II}) and the sulfate anion acts as a bridge ligand between two Cu(II) (Fig. 20e). Both Cu(II) metal center showed octahedral coordination geometry, in which all the four equatorial positions are coordinated by **bix** and axial positions are coordinated by sulfate in bidentate μ_2 fashion bridge between two Cu(II). The infinite polymerization of *trans* and *gauche* conformations of **bix** resulted in a 2D layer of (4,4) topology (A layer and B layer) having a space group symmetry of *c2mm* and *p4gm*, respectively. The A and B layers are stacked along [001] and [100] direction via ABAB sequence and such layers undergo inclined polycatenation (Fig. 20f). Further the sulfate anion bridge the A and B 2D layers which lead to the formation of an unprecedented 3D CP having a $4^8\cdot6^7$ topology which confirms the self-catenation or poly-knotting in the network.

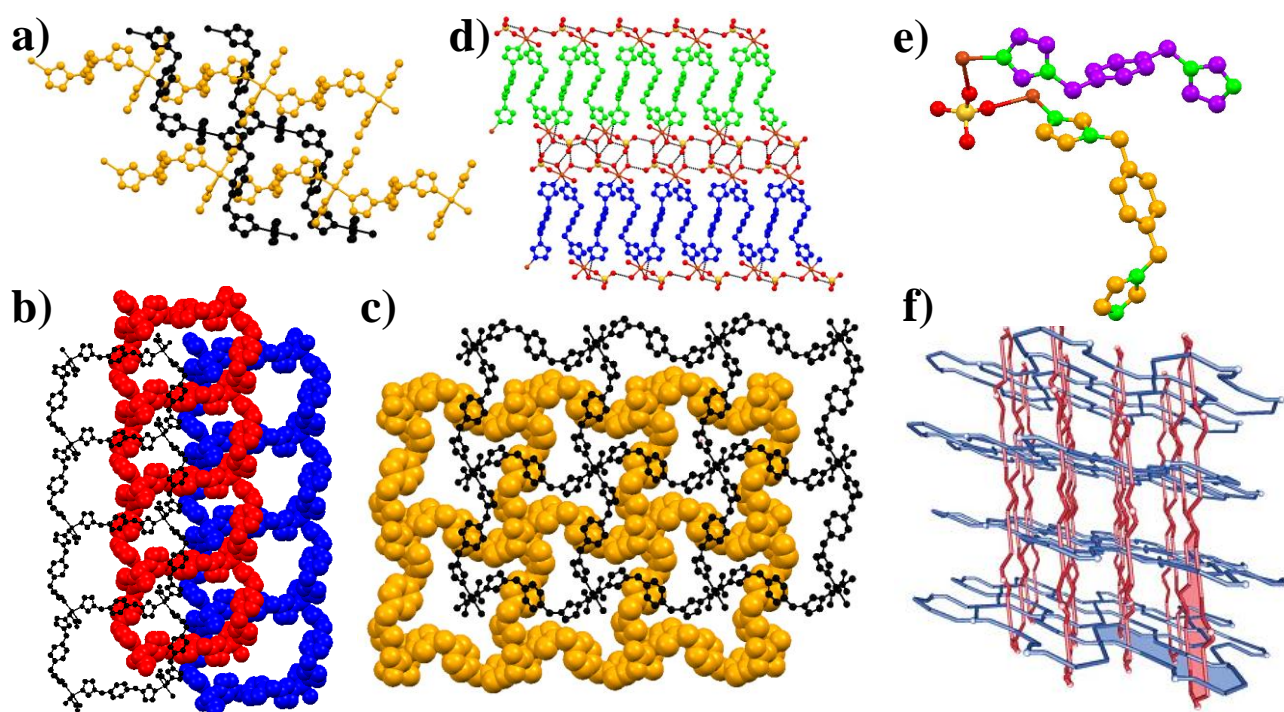


Fig. 20: a) parallel packed 1D CP chains (shown in orange and black) in **22**; b) ABAB stacking of 1D CP ladder in **23**; c) offset packing of 2D CP (4,4) grids in **24**; d) 1D chains (shown in blue and green color) in CP **25** and its hydrogen bonding through sulfate and water; e) asymmetric unit of CP **26**; f) inclined polycatenation of A (red) and B (blue) 2D layers in CP **26**. Fig. 20f is reprinted from ref. 42 with permission. Copyright 2004, Royal Society of Chemistry.

2.6. Fe-bix and Mn-bix CPs

Although examples of **bix** containing CP with Iron or Manganese these metals are scarce, some interesting structures can be found. Recently a Fe(II) CPs namely $[\{\text{Fe}(\text{bix})_2(\text{NCS})_2\} \cdot \text{H}_2\text{O}]_\infty$ (**27**) was reported by Beheshti *et al.*⁴³ The SXRD analysis revealed a 2D CP with square grid (4, 4) structure (similar structure to **24** – Fig. 20c) packed in ABCDE...ABCDE fashion, supported by various non-covalent interactions. As expected, Fe(II) metal center exhibits distorted octahedral coordination geometry and the **bix** ligand adopt *trans* conformation in the crystal structure. The equatorial positions of Fe(II) are occupied by **bix** and the axial ones by NCS^- . In that manner a FeN_6 chromophore, one of the primary requirement for spin-crossover (SCO) materials was formed.⁴⁴ However, SCO properties of **27** have been not yet reported.

Concerning manganese derivatives, Carlucci *et al.* reported three Mn(II) CPs namely $[\{\text{Mn}_2(\text{bix})_3(\text{NO}_3)_4\} \cdot 2\text{CHCl}_3]_\infty$ (**28**), $[\{\text{Mn}(\text{bix})_{1.5}(\text{NO}_3)_2\}]_\infty$ (**29**) and $[\{\text{Mn}(\text{bix})_2(\text{NO}_3)_2\}]_\infty$ (**30**).⁴⁵ The reaction of **bix** and $\text{Mn}(\text{NO}_3)_3$ in 1 : 3 metal-to-ligand ratio in EtOH- CHCl_3 (by slow diffusion method) at 34°C resulted in the concomitant crystallization of **28** as major product of the supramolecular isomers and **29**. Interestingly, when the amount of **bix** is reduced to 1 : 1.5 metal-to-ligand ratio resulted exclusively in **29**. On the other hand if the 1:3 ratio is maintained but the temperature is increasing to 60°C, and further slow evaporation lead to the thermodynamic product **30**. The SXRD analysis of **28** revealed two different (crystallographically independent) metal-organic motifs in which the Mn(II) exhibit seven coordinated pentagonal-bipyramidal geometry with a N_3O_4 donor set. The equatorial coordination sites are occupied with two nitrate anions (bidentate in a chelate mode) and one **bix** ligand, while the axial positions are bond by **bix** ligands. The **bix** ligand adopted a *trans* conformation in the two motifs. In motif 1, the coordination polymerization of **bix** with Mn(II) lead to formation of a 2D nano-porous (13.05 × 29.52 Å) brick wall shaped layers having a 6^3 topology (Fig. 21a), and in motif 2 the combination of **bix** and Mn(II) resulted in a 1D ladder structure having rhombic shaped grids (Fig. 21b). However, the nano-pores are blocked due to interpenetration of 2D layers through inclined polycatenation with the 1D ladders via topological Hopf links (1D + 2D) and resulted in a 3D supramolecular network. Hopf link is a terminology used to define the single interpenetration of two distinct circuits in the network, in order to achieve close packing to fill the void space in the crystal lattice. Even after such interpenetration some voids with enclatrate CHCl_3 solvent molecules were present (Fig. 21c).

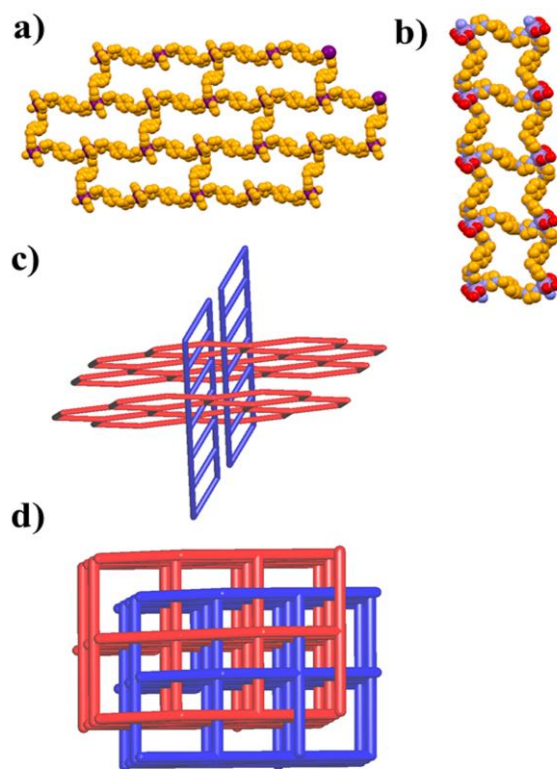


Fig. 21: 2D layer brick wall shaped CP **28** displaying 6^3 topology of network; b) 1D ladder CP **29**; c) TOPOS view of polycatenation in **29** (the 2D and 1D motifs are shown on red and blue color); d) 2-fold interpenetrated 3D CP network in **30**.

In contrast to the structure of **28**, the supramolecular isomer **29** showed a 1D ladder like metal-ligand coordination structure could be due to the presence of only one motif. On the other hand the structure of thermodynamically stable CP **30** was a 3D CP having CdSO_4 topology ($6^5 \cdot 8$ cds) and showed 2-fold interpenetration. The metal center Mn(II)

showed distorted octahedral coordination geometry in which equatorial and axial coordination sites are occupied by N atoms of **bix** and O atoms of nitrate, respectively. Thus the infinite coordination of **bix** (*trans* conformation) resulted in the 3D structure in **30**.

Can we control the supramolecular architecture of crystalline CPs built from **bix**?

All above examples showed the progress and achievements of the structural and coordination chemistry of crystalline CPs built from **bix** ligand and M(I)/M(II) (M = Ag(I), Zn(II), Cd(II), Co(II), Cu(II), Fe(II) and Mn(II)) salts. Single crystal X-ray structures of the CPs **1-30** discussed here provide us not only to understand their 3D structures, but also offer an invaluable insights of the coordination ability of **bix** and the diversity in structure and topology of different combinations metal-ligand. The diversity in the structure is directed related to the effect of the coordination geometry of M(I)/M(II), the type of counter- anion, the metal-to-ligand ratio, the reaction conditions and the conformation of **bix**. In Table 1 are listed all the examples discussed summarizing the specific reaction conditions and the structural parameters of the resulting materials. The reaction condition (RT in **1** and HT in **1a**), coordination geometry of metal ion (Tp in **1** and linear in **1a**) and conformation of **bix** (*gauche* + *trans* in **1** and only *trans* in **1a**) are the main factors that determine a 1D Ag(I) CP having alternate ring and rod topology in **1** and 1D Ag(I) *zigzag* CP having only rod topology in **1a**. The change of trigonal planar shaped anion NO₃⁻ in **1** and **1a** with linear shaped CN⁻ and spherical shaped I⁻ lead to 2D CP sheet structure in **2** and **3**. Concerning Zn(II) metal center, all the examples showed Td coordination geometry for the metal node (**4-9**); while the counter-anions (NO₃⁻ in **4** and **4a**; SO₄²⁻ in **5**, Br⁻ in **6**, Cl⁻ in **7**, HPO₄²⁻ in **8**, HPO₃²⁻ in **9**), metal-to-ligand ratio (1 : 0.5 in **8** and **9**, 1 : 1 in **6** and **7**; 1 : 1.5 in **5**; 1 : 2 in **4** and **4a**), reaction condition (RT in **4**, **4a** and **5**; HT in **6-9**) and conformation of **bix** (*gauche* + *trans* in **4** and **4a**; *gauche* only in **5** and **6**; *trans* only in **8** and **9**) are effected the final structure of Zn(II) CPs: 1D CPs in **5** and **7**, 2D CP sheets in **4**, **4a** and **8**, 3D CP in **9**, and metalamacrocycle in **6**. Similar structural diversities is also observed in the Cd(II), Co(II) and Cu(II) derivatives (**10-26**). Metal variation in the nitrate salts of M(I)/M(II) (M = Ag(I), Zn(II), Cd(II), Cu(II) and Mn) and its effect on the final structures of CPs such as **1**, **1a** (1D CP), **4**, **4a** (2D CP), **11** (3D CP), **12** (1D CP), **13** (2D), **24** (2D CP) and **28**, **29** and **30** also provide us a clear picture of uncertainty in the structure of kinetic products of CPs. Such un-predictability in the structures of CPs of **bix** can be overcome in some extent by using crystal engineering concepts.⁴⁶ The unexpected conformations of **bix** due to its flexibility helped us to understand topologies such as polyrotaxane in **1**, **1a**, **5**, **14** and **18**, polycatenation in **26** and **29**, different interpenetration of 2D, 3D CPs **2**, **4a**, **10**, **17** and **30**. Thus with the precedent examples of different combination of metal salts and reaction conditions and great diversity of possible structures we can understand a rational design of the final structure by playing with the metal-to-ligand ratio, solvent, temperature and reaction conditions.

Table 1[#]

CP	SG	CG	CL	M : L_R	M : L_CP	Anion	RC	Structure and property	REFCODE	Ref.
$[\{\text{Ag}_2(\text{bix})_3\} \cdot (\text{NO}_3)_2]_\infty$ (1)	$P2_1/n$	TP	2 <i>gauche</i> , 1 <i>trans</i>	1 : 1.7	1 : 1.5	NO_3^-	RT, H_2O , MeOH	Two 1D CPs, further undergo polycatenation (1D \rightarrow 2D)	RIZZEF	19
$[\{\text{Ag}_2(\text{bix})_2\} \cdot (\text{NO}_3)_2 \cdot 2\text{H}_2\text{O}]_\infty$ (1a)	$P\bar{1}$	linear	2 <i>trans</i>	Data not available	1 : 1	NO_3^-	Data not available	Two 1D wavy CPs, further undergo polycatenation	MAZBUL	21
$[\{\text{Ag}_4(\text{CN})_4(\text{bix})_2\}]_\infty$ (2)	$P\bar{1}$	TP	<i>gauche</i>	1.9 : 1	2 : 1	CN^-	HT, CH_3CN	2D CP sheet, further undergo 2D interpenetration	PEVB EY	22
$[\{\text{Ag}_4\text{I}_4(\text{bix})\}]_\infty$ (3)	$P\bar{1}$	Td	<i>anti</i>	2 : 1	1 : 1	I^-	HT, H_2O , MeOH, KI	2D CP corrugated sheet,	QATXOA	23
$[\{\text{Zn}(\text{bix})_2\}(\text{NO}_3)_2 \cdot 4.5\text{H}_2\text{O}]_\infty$ (4)	$P\bar{1}$	Td	<i>trans</i> , <i>gauche</i>	1 : 2.9	1 : 2	NO_3^-	RT, H_2O , MeOH	2D CP, undergo polycatenation	NEBSUI	24
$[\{(\text{Zn})_2(\text{bix})_4\} \cdot (\text{NO}_3)_4 \cdot 5\text{H}_2\text{O}]_\infty$ (4a)	$P\bar{1}$	Td	<i>trans</i> , <i>gauche</i>	1 : 2	1 : 2	NO_3^-	RT, H_2O , MeOH	2D CP corrugated sheet, further undergo parallel interpenetration	CEHNEJ	25
$[\{\text{Zn}_2(\text{bix})_3(\text{SO}_4)_2\} \cdot 8\text{H}_2\text{O}]_\infty$ (5)	$P2_1/n$	Td	2 <i>gauche</i>	1 : 2 or 1 : 1.5	1 : 1.5	SO_4^{2-}	RT, H_2O -Acetone	1D wavy CP, further undergo parallel interlocking to form a 2D polyrotaxane sheet	FAZZOW	26
$[\{\text{Zn}_2(\text{bix})_2(\text{Br})_2\}]_\infty$ (6)	$C2/m$	Td	2 <i>gauche</i>	1 : 1	1 : 1	Br^-	HT, 70°C, DMF, MeOH	metallo-macrocyle, further packed into a 3D hydrogen bonded porous network	UGOJIL	27
$[\{\text{Zn}(\text{bix})(\text{Cl})_2\}]_\infty$ (7)	$Pbcn$	Td	<i>trans</i>	1 : 1	1 : 1	Cl^-	HT, 140°C, H_2O -EtOH	1D CP, further assembled to 2D H-bonded sheet network and finally undergo orthogonal packing.	ZANVAN	28
$[\{\text{Zn}_2(\text{HPO}_4)_2(\text{bix})\} \cdot 2\text{H}_2\text{O}]_\infty$ (8)	$P\bar{1}$	Td	<i>trans</i>	1 : 1	2 : 1	HPO_4^{2-}	HT, 130°C, H_2O	2D CP	YAHMAW	29
$[\text{Zn}(\text{HPO}_3)(\text{bix})_{0.5}]_\infty$ (9)	$P2_1/c$	Td	<i>trans</i>	1 : 0.5	1 : 0.5	HPO_3^{2-}	HT, 125°C, H_2O	3D CP		30
$[\{\text{Cd}(\text{bix})_3\} \cdot (\text{ClO}_4)_2 \cdot 0.7\text{MeOH}]_\infty$ (10)	$R\bar{3}$	O_h	<i>trans</i>	1 : 4	1 : 3	ClO_4^-	RT, MeOH, TEOF	3D CP having α -polonium topology, further interpenetrated into 3-fold	HUKQUZ	31
$[\{\text{Cd}(\text{bix})_3\} \cdot (\text{NO}_3)_2]_\infty$ (11)	$P\bar{1}$	O_h	<i>trans</i>	1 : 3	1 : 3	NO_3^-	RT, H_2O , MeOH	3D CP having α -polonium topology, 3D CP having α -polonium topology	HUKRAG	31
$[\text{Cd}(\text{bix})(\text{NO}_3)_2(\text{DMF})_2]_\infty$ (12)	$C2/c$	O_h	<i>trans</i>	2 : 1	1 : 1	NO_3^-	HT, 100°C, DMF, Cl-AcAcid	1D zig-zag CP, further extend to 2D hydrogen bonded network	HOMQEH	32
$[\text{Cd}(\text{bix})_2(\text{NO}_3)_2]_\infty$ (13)	$P2_1/c$	O_h	<i>trans</i>	1 : 2	1 : 2	NO_3^-	RT, H_2O , MeOH	2D CP with (4, 4) grid like architecture, further packed in an off-set fashion supported by H-bonding	RAJFEP	33
$[\{\text{Cd}_2(\text{bix})_3(\text{SO}_4)_2\}]_\infty$ (14)	$P2_1/n$	Tbp	<i>trans</i> , <i>gauche</i>	1 : 2	1 : 1.5	SO_4^{2-}	RT, H_2O , Acetone	1D CP chain with alternate ring and rod shaped topology which extend to 2D CP via SO_4^{2-} bridging (μ_2 fashion), can be called as “self-threaded” 2D CP	FAZZUC	26
$[\{\text{Cd}_2(\text{bix})_2(\text{H}_2\text{O})_4(\text{SO}_4)_2\} \cdot (\text{bix})]_\infty$ (15)	$P2_1/c$	O_h	<i>trans</i>	1 : 2 or 1 : 1.5	1 : 1	SO_4^{2-}	RT, H_2O , Acetone	2D CP with (4, 4) layers of rhombic meshes.	FEBBAQ	34

CP	SG	CG	CL	M : L_R	M : L_CP	Anion	RC	Structure and property	REFCODE	Ref.
$[\{\text{Cd}(\text{bix})_{0.5}(\text{H}_2\text{O})_2(\mu_3\text{-SO}_4)\} \cdot \text{H}_2\text{O}]_\infty$ (16)	$P2_1/c$	O _h	<i>trans</i>	Data not available	1 : 0.5	SO ₄ ²⁻	HT, H ₂ O, MeOH	3D open framework structure, whose cavities are occupied with solvated water molecules. Room temperature photoluminescence	YEVPAR	34
$[\{\text{Cd}_2(\text{bix})_4(\text{SCN})_4\}]_\infty$ (17)	$P\bar{1}$	O _h	<i>gauche</i> , the imidazole N donor atoms are <i>trans</i> to each other	1 : 1	1 : 2	SCN ⁻	HT, 120°C, H ₂ O	3D CP having topology, further interpenetrated into 3-fold	ZIQCEJ	35
$[\{\text{Co}(\text{bix})_2(\text{H}_2\text{O})_2\} \cdot (\text{SO}_4) \cdot 7\text{H}_2\text{O}]_\infty$ (18)	$C2/c$	O _h	<i>trans, gauche</i>	1 : 2	1 : 2	SO ₄ ²⁻	RT, H ₂ O-acetone	A combination of 3D CP having a the (6 ⁵ .8) CdSO ₄ topology and 1D looped chain CP, both are entangled via catenation (1D + 3D)	ATEYED	36
$[\{\text{Co}(\text{bix})(\mu_2\text{-SO}_4)(\text{H}_2\text{O})_2\}]_\infty$ (19)	$Pbcm$	O _h	<i>gauche</i>	1 : 2	1 : 1	SO ₄ ²⁻	RT, MeOH-CHCl ₃	2D corrugated sheet CP and the packing of sheets along the b-axis which showed nano-porous structure	ATEYIH	36
$[\{\text{Co}(\text{bix})_3\} \cdot 2\text{OH} \cdot \text{CH}_3\text{OH} \cdot 3\text{H}_2\text{O}]_\infty$ (20)	$C2/c$	O _h	<i>trans</i>	1 : 3	1 : 3	OH ⁻	HT, reflex temperature, H ₂ O, MeOH	3D coordination polymer having open diamond-shaped cavities which are filled guest OH ⁻ , solvated MeOH and H ₂ O. Weak antiferromagnetic	VADWON	37
$[\{\text{Co}(\text{bix})_{0.5}(\text{HPO}_3)_3\} \cdot 3\text{H}_2\text{O}]_\infty$ (21)	$P2_1/n$	Td	<i>trans</i>	1 : 1	1 : 0.5	HPO ₃ ²⁻	HT, 90°C, H ₂ O, DMF	2D CP showed weak interactions between the Co ^{II} centers	YECQUT	38
$[\text{Cu}_2(\text{ac})_4(\text{bix})_2]_\infty$ (22)	$P1$	O _h	<i>trans</i>	1 : 1	1 : 1	ac ⁻	HT, reflex, MeOH	1D zig zag CP chain, further extended to 3D hydrogen bonded network	FARVAW	39
$[\{\text{Cu}_2(\text{CO}_3)_2(\text{bix})_3\} \cdot (\text{bix}) \cdot 10\text{H}_2\text{O}]_\infty$ (23)	$P\bar{1}$	spy	<i>trans, strained-gauche</i>	1 : 1	1 : 1.5	CO ₃ ²⁻	RT, Magnetic stirring, H ₂ O	1D CP having ladder structure, further self-assembled via non-bonded interactions	EFULUN	40
$[\{\text{Cu}(\text{NO}_3)_2(\text{bix})_2\} \cdot \text{H}_2\text{O}]_\infty$ (24)	$P\bar{1}$	O _h	<i>trans</i>	Data not available	1 : 2	NO ₃ ⁻	Data not available	2D CP having a (4,4) square grid structure, packed via ABAB... fashion.	DECCOE	41
$[\{\text{Cu}(\text{bix})(\text{H}_2\text{O})_3(\text{SO}_4)\} \cdot \text{H}_2\text{O}]_\infty$ (25)	$P\bar{1}$	O _h	<i>trans</i>	1 : 1	1 : 1	SO ₄ ²⁻	RT, H ₂ O-acetone	1D highly undulated CP chain, further extend to 2D hydrogen bonded sheet.	EWAXOP	42
$[\{\text{Cu}(\text{bix})_2(\text{SO}_4)\} \cdot 7.5\text{H}_2\text{O}]_\infty$ (26)	$C2/c$	O _h	<i>trans, gauche</i>	1 : 3	1 : 2	SO ₄ ²⁻	RT, H ₂ O-acetone	3D CP having a 4 ⁸ .6 ⁷ topology	EWAXUV	42
$[\{\text{Fe}(\text{bix})_2(\text{NCS})_2\} \cdot \text{H}_2\text{O}]_\infty$ (27)	$P\bar{1}$	O _h	<i>trans</i>	1 : 2	1 : 2	NCS ⁻	RT, H ₂ O-EtOH	2D CP with square grid (4, 4) structure	MISPEL	43
$[\{\text{Mn}_2(\text{bix})_3(\text{NO}_3)_4\} \cdot 2\text{CHCl}_3]_\infty$ (28)	$P\bar{1}$	Pbp	<i>trans</i>	1 : 3	1 : 1.5	NO ₃ ⁻	EtOH-CHCl ₃ at 34°C	Interpenetrated 2D layers through inclined polycatenation with the 1D ladders via topological Hopf links (1D + 2D)	TIVYED	45
$[\{\text{Mn}(\text{bix})_{1.5}(\text{NO}_3)_2\}]_\infty$ (29)	$P\bar{1}$	Pbp	<i>trans</i>	1 : 3	1 : 1.5	NO ₃ ⁻	EtOH-CHCl ₃ at 34°C	1D CP having ladder structure, further interact with each other by weak interactions.	TIVYIH	45
$[\{\text{Mn}(\text{bix})_2(\text{NO}_3)_2\}]_\infty$ (30)	$P\bar{1}$	O _h	<i>trans</i>	1 : 3	1 : 2	NO ₃ ⁻	EtOH-CHCl ₃ at 60°C	3D CP having CdSO ₄ topology (6 ⁵ .8 cds) and showed 2-fold interpenetration.	TIVYON	45

#CP – Coordination polymer; SG – Space group; CG – Coordination geometry; CL – Conformation of bix; M : L_R – Metal : ligand ratio during reaction; M : L_CP – Metal : ligand ratio of CP; RC – Reaction condition and solvent used; Ref – reference number; TP – Trigonal planar; O_h – Octahedral; Tbp – Trigonal bi-pyramidal; spy – Square pyramidal; Pbp – Pentagonal bi-pyramidal; RT – Room temperature; HT – High temperature.

2. Amorphous CPs

Amorphous CPs are materials formed by the self-assembly of metal ion and organic ligand which results in a non-regular packed array. As a result, the structure of these materials cannot be elucidated through X-ray diffraction techniques. When amorphous CPs are synthesized at the nanoscale (1 nm –few hundred nm) they are called nanoscale coordination polymers (NCPs) or coordination polymer particles (CPPs) and usually exhibits spherical morphology. Typically, CPPs are synthesized by mixing metal ion and organic ligand in presence of a poor solvent (a solvent that induce CPs precipitation), so that CPs precipitate immediately as spherical shaped nanoparticles. The resulting spherical shape is due to its tendency to minimize the interfacial free energy between the surface of the CPPs and solvent. It is worthwhile to mention here that, the crystalline counterpart of CPPs are known as nanoscale metal-organic frameworks (NMOFs) in which the building blocks are self-assembled and packed in a regular array as unit cells. Therefore the exact solid state structure, composition and packing of NMOFs with atomic resolution can be expose by single and powder X-ray diffraction, which will support researchers to plan a new design strategy and also analyse the structure-property correlation.

Almost a decade ago (2005), the first example of amorphous CPP was reported by Mirkin *et al.*⁴⁷ They reported a series of CPPs by reacting a metalloligand derived from a homochiral carboxylate-functionalized bis-metallotridentate Schiff base (BMSB) and M(II) acetates (M = Zn, Cu, Ni) in polar solvent like pyridine (Fig. 22a). In contrast to the above mentioned method, a poor non-polar solvent (diethyl ether or pentane) was added to the reaction mixture, which resulted in the spontaneous precipitation of CPP as particles of diameters of a few hundred nanometres (Fig. 22b). Interestingly, at initial stage small particles aggregates form intermediate clusters which further coalesce and anneal into uniform and smooth nanoparticles. In the same year, Wang *et al.* reported the synthesis of a platinum-based amorphous CPPs by mixing the metal salt (H_2PtCl_6) with organic linker p-phenylenediamine, using different molar ratio in aqueous solutions at room temperature; the resultant CPP showed unprecedented mono-dispersed nanoparticles in aqueous solvents having a spherical morphology with an average diameter of 420 nm (Fig. 22c).⁴⁸ This coordination-induced assembly process proceed repeatedly until the depletion of reactants in the solution, resulting in the formation of large coordination polymers. However, the detailed formation mechanism was not clear. Later, Sweigart *et al.* also explored the synthesis and precipitation of CPPs in poor solvents by self-assembling of $[(\eta^6\text{-}1,4\text{-hydroquinone})\text{Rh}(\text{cod})]^+$ complexes linked by Al(III). The coordination polymer resulted in spherical nanoparticles having an average diameter of 340 nm (Fig. 22d). Interestingly these CPPs showed catalysis properties for the stereoselective polymerization of phenylacetylene.⁴⁹ In 2008, Lin *et al.* reported an unprecedented CPPs built from an anticancer prodrug disuccinatocisplatin (DSCP) and Tb^{III} .⁵⁰ The authors described a general strategy to formulate highly degradable nanoparticles based on Pt-containing nanoscale coordination polymers. The encapsulation of the CP in shells of amorphous silica allows to control the release of the Pt drug. This work demonstrated the potential application of these CPPs as effective delivery vehicles for a variety of biologically and medically important cargoes such as therapeutic and imaging agents (Fig. 22e).

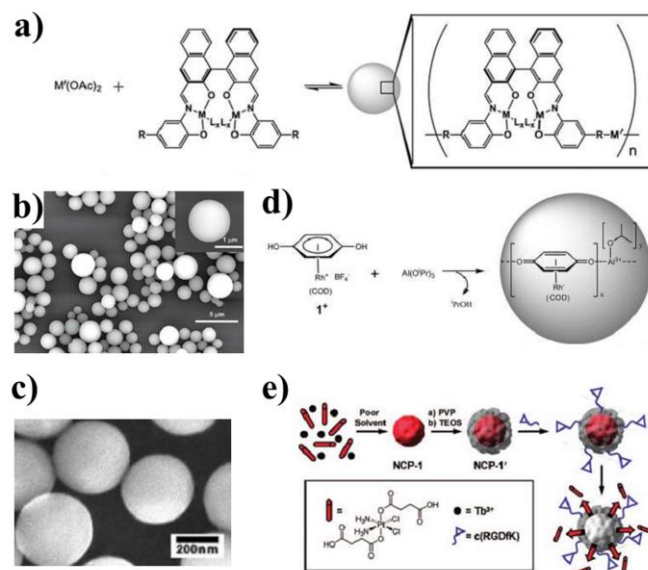


Fig. 22: a) CPP built from bis-metallo-tridentate Schiff base (BMSB) and M(II) acetates ($M = \text{Zn, Cu, Ni}$); b) SEM image of Zn-BSM-Zn CPPs (inset – high resolution image); c) SEM image of CPP obtained from H_2PtCl_6 and p-phenylenediamine; d) schematic representation of the synthesis of organometallic CPP catalyst; e) schematic representation of Pt(IV) prodrug-CPP formation, coating, functionalization and drug delivery (inset: the Pt(IV) prodrug DSCP used as a building block of the CPPs). Fig. 22a-b are reprint from ref. 47 with permission. Copyright 2005, Nature Publishing Group. Fig. 22c, 22d and 22e are reprinted from ref. 48, 49 and 50 respectively with permission. Copyright 2005, 2006 and 2008 American Chemical Society.

Since these seminal works, an intense research activities concerning design and synthesis of CPPs⁵¹ was developed in the last decade due to their enormous potential applications such as in heterogeneous catalysis,⁴⁹ spin-crossover,^{52,53} bio-sensing and multimodal imaging⁵⁴ or drug delivery.⁵⁵ In this scenario, the flexibility of the **bix** ligand offers a great opportunity to exploit its coordination and structural properties for building functional coordination polymers. As the main focus of this perspective is CPs contained **bix** as polymerizing ligand, we will discuss in more detail the amorphous CPPs built from only **bix** ligand or where **bix** is the main ligand. One of the earlier example of **bix**-based amorphous CPPs was the Zn(II)-**bix** CPPs synthesized by mixing $\text{Zn}(\text{NO}_3)_2$ and **bix** by using “poor solvent precipitation” approach.⁵⁶ The colloid solution of Zn-Bix CPP in EtOH showed chemical stability for more than one month; from Scanning (SEM) and transmission (TEM) electron microscopy images of the colloid revealed the spherical shaped morphology having a uniform diameters in the range 100–1500 nm. In fact the size of the Zn-bix CPPs can easily tune controlling the concentration of precursors $\text{Zn}(\text{NO}_3)_2$ and **bix**. These nanoparticles exhibit fluorescent properties and showed a blue emission at 405 nm (excited at 355 nm). The encapsulation capability of CPPs was nicely demonstrated by Inhar et al.,⁵⁶ by reacting $\text{Zn}(\text{NO}_3)_2 \cdot 6\text{H}_2\text{O}$ and **bix** in presence of different guest species. The extended coordination polymerization followed by fast precipitation with a poor solvent, resulted in the self-assembly of cross-linked sub- micrometre functional metal–organic Zn-**Bix** spheres along with encapsulation of guest species (i.e. magnetic nanoparticles, fluorescent organic dyes, quantum dots) (Fig. 23).

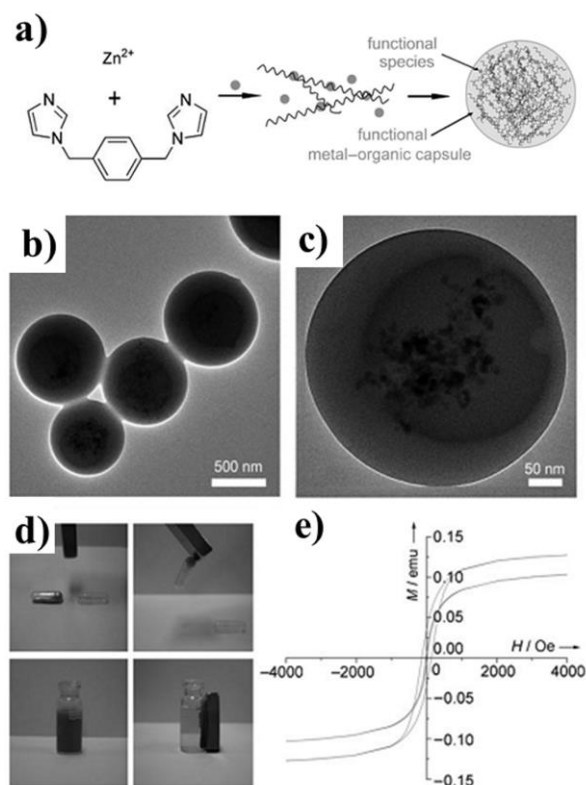


Fig. 23: Schematic representation of encapsulation of guest species within the CPPs; b) and c) TEM image of iron oxide nanoparticles encapsulated in Zn-bix CPPs; d) photographs showing the attraction of iron oxide nanoparticles/Zn(bix) nanospheres to a magnet; e) Magnetic hysteresis loop measured at room temperature and at 10K. Fig. 23 are reprint from ref. 56 with permission. Copyright 2009, Wiley-VCH Verlag GmbH & Co. KGaA, Weinheim.

Encapsulation of two components (or multiple substances) was also explored by following *in situ* formation of Zn-bix in presence of a mixture of active species (Fig. 24). For example, the co-encapsulation of quantum dots and fluorescein with Zn-bix (QD-fluorescein@Zn-bix) offers a multifunctional optical device containing three fluorescent emissive probes which covers the entire visible spectrum by combining intrinsic fluorescence properties of the Zn-bix CPP and those characteristics of the encapsulated QD and fluorescein (Fig. 24d-f). Following a similar synthetic methodology, Zn(bix)spheres that encapsulate luminescent QDs and magnetic iron oxide nanoparticles were also fabricated (Fig. 24g-i).

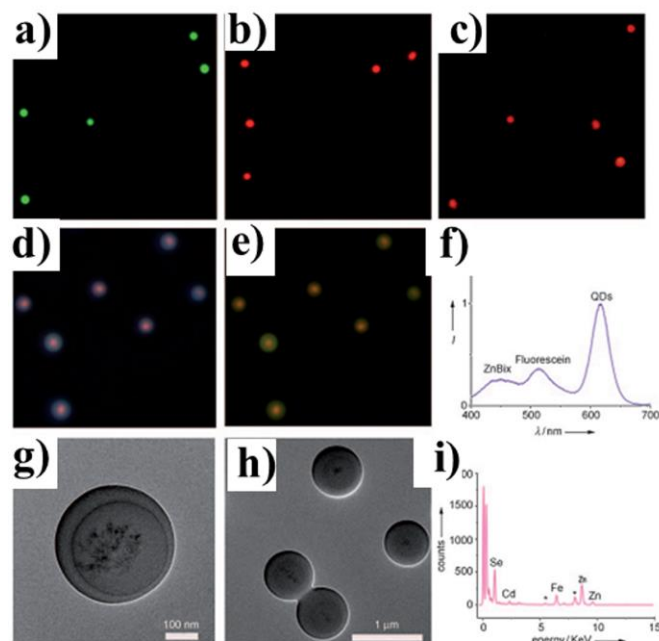


Fig. 24: a)-c) Fluorescence optical microscope images of fluorescein ($\lambda_{exc} = 450\text{--}490\text{ nm}$, $\lambda_{em} > 515\text{ nm}$), rhodamine B ($\lambda_{exc} = 540\text{--}552\text{ nm}$, $\lambda_{em} > 590\text{ nm}$) and QDs ($\lambda_{exc} = 540\text{--}552\text{ nm}$, $\lambda_{em} > 590\text{ nm}$) encapsulated in Zn-Bix CPP; d) e) Fluorescence optical microscope images of QD-fluorescein@Zn-bix CPP collected at various conditions; f) Fluorescence emission spectra of QD-fluorescein@Zn-bix CPP measured at $\lambda_{ex} = 355\text{ nm}$, where both the CPP matrix and the encapsulated fluorophores absorb; g,h) High-resolution TEM images of QDs/iron oxide nanoparticles/Zn(bix) spheres. i) RX-EDX spectrum of QDs/iron oxide nanoparticles/Zn(bix) spheres. Fig. 24 are reprint from ref. 56 with permission. Copyright 2009, Wiley-VCH Verlag GmbH & Co. KGaA, Weinheim.

Encouraged by these results, Inhar et al developed a Zn-bix CPP host for the encapsulation of anti-cancer drugs such as Doxorubicin (DOX), SN-38, camptothecin (CPT) and daunomycin (DAU) (Fig. 25).⁵⁷ Due to their intrinsic fluorescent emission, the encapsulation drugs can be easily monitored by fluorescence microscopy. In the same way, fluorescence spectroscopy was used to study the drug release profiles of different drug-Zn(bix) colloidal solutions (Fig. 26a). Similar to other encapsulating systems, release profiles can be attributed to both desorption and diffusion of drug as well as to the gradual erosion of Zn(bix) spheres as observed by SEM (Fig. 26b). Complementary in vitro studies demonstrated the potential of CPPs for drug delivery and anticancer efficacies (Fig. 26 c-d).

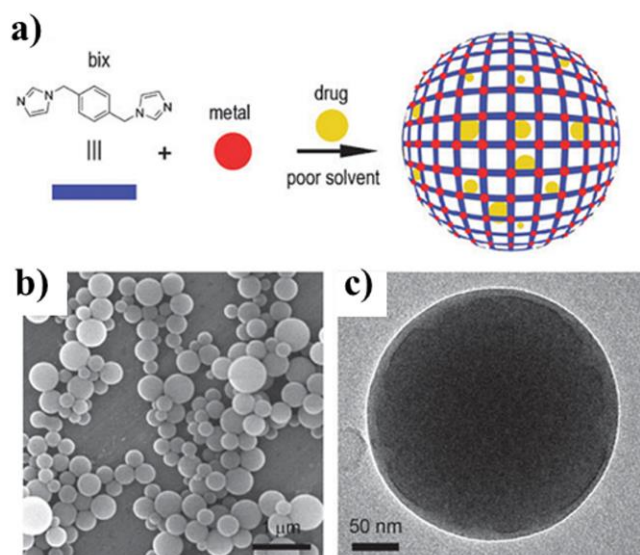


Fig. 25: a) Schematic representation of the encapsulation of drugs within Zn-Bix CPP matrix; b) SEM and b) TEM images of drug-encapsulated CPP. Fig. 26 are reprint from ref. 57 with permission. Copyright 2010, The Royal Society of Chemistry.

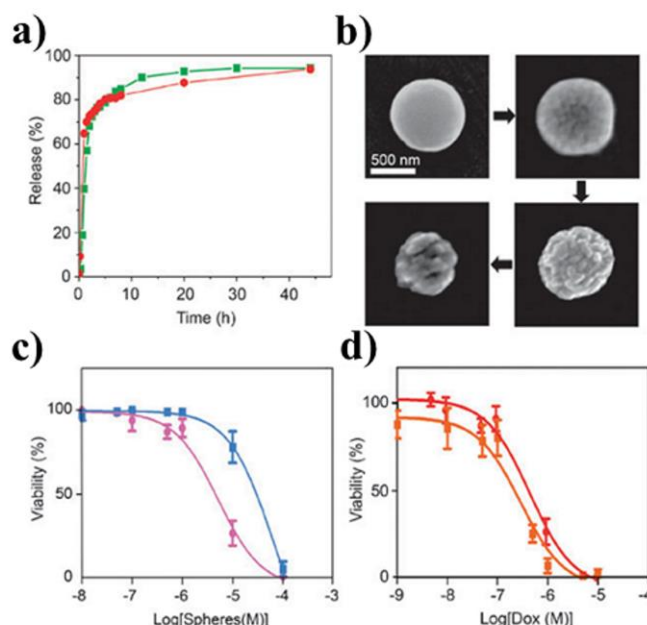


Fig. 26: a) In vitro release profile of DOX and SN-38 from DOX-Zn(bix) (dot, red) and SN38-Zn(bix) (square, green) spheres incubated at physiological condition; b) SEM images of DOX-Zn(bix) CPPs taken at 1, 4, 8, and 24 hours; c) In vitro cytotoxicity assay curves after 24 h for HL60 cells obtained by plotting the cell viability % against the Zn(bix) (square, blue) and DOX/Zn(bix) (dot, pink) concentration and (d) the DOX release from DOX/Zn(bix) spheres (dot, red) and DOX (square, orange) concentration. Fig. 26 are reprint from ref. 57 with permission. Copyright 2010, The Royal Society of Chemistry.

In a subsequent work, Che *et al.* explored the capability of Zn-bix CP matrix to act as a protective coating for anti-cancer drugs which are physiologically unstable, and thus designed and synthesized core-shell CPPs.⁵⁸ The core belongs to the “drug-metal” coordination polymer nanoparticle and the shell represent the Zn-bix CPP matrix. The drugs such as S-(N-p-chlorophenyl-N-hydroxycarbonyl)glutathione (CHG), methotrexate (MTX) and Calcein were used to react with biocompatible metal ions Fe(III) and Zn(II), by poor solvent precipitation method (Fig. 27a). SEM images reveal that the cores have a spherical morphology with smooth surfaces with an average diameters of ~ 155, ~ 145, ~ 160 and ~ 115 nm for CHG-Fe, MTX-Zn, MTX-Fe and Calcein-Fe, respectively which further increase its diameter to ~ 225, ~ 210, ~ 235 and ~ 180 nm, when it was covered by Zn-bix shell (Fig. 27b-c). Interestingly, the

core-shell CPP not only improved the stability under physiological conditions, but also enabled pH-triggered drug release.

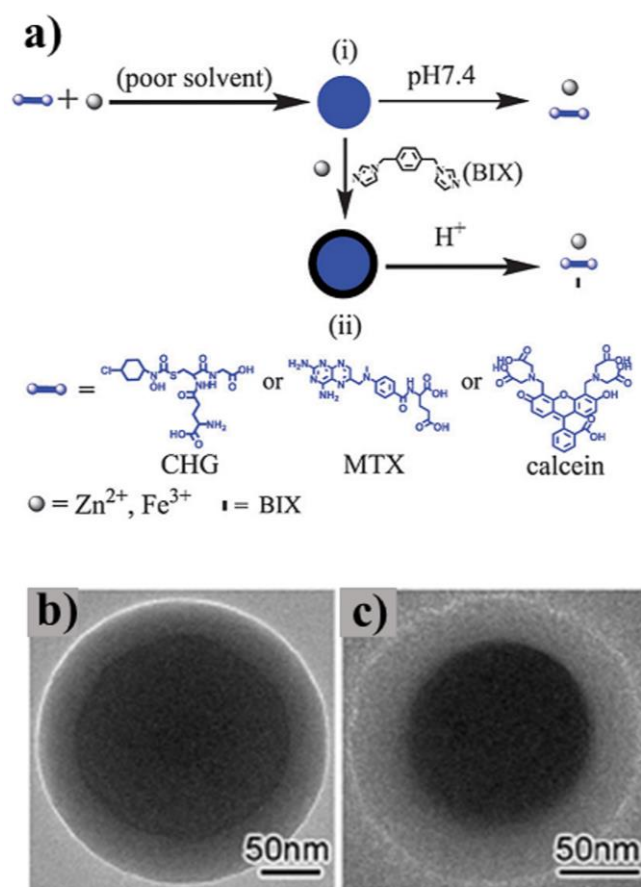


Fig. 27: Schematic representation of the synthesis of core-shell CPP; b) TEM image of MTX-Fe-BIX-Zn shell CPP; c) TEM image of Calcein-Fe@BIX-Zn. Fig. 27 are reprint from ref. 58 with permission. Copyright 2012, The Royal Society of Chemistry.

The in vitro studies determined that core-shell CPPs protect the drug and effectively deliver intracellularly exhibiting a higher cytotoxicity against HeLa cells than core CPPs and free drug.

Recently, Deng *et al.* reported a Zn-bix CPP with encapsulated rhodamine B (RhB) namely RhB/Zn(bix) CPP by exploiting the stability of the particles in EtOH.⁵⁹ Nevertheless the addition of water into the ethanolic solution of RhB/Zn(bix) CPP resulted in the release of encapsulated RhB and the break of Zn(Bix) coordination network. Interestingly, variations in the solvent display the color and strengthening of fluorescence of RhB. Thus the stable and unstable behaviour of Zn-bix CPP in EtOH and H₂O, respectively was utilized to develop a novel colorimetric and fluorescent dual mode sensing to sense the alcoholic strength in commercial spirit samples. The sensor exhibits naked eye detection of % of alcohol within a wide linear range from 20 to 100% vol and by monitoring the increase o fluorescent intensity of the released RhB (Fig. 28).

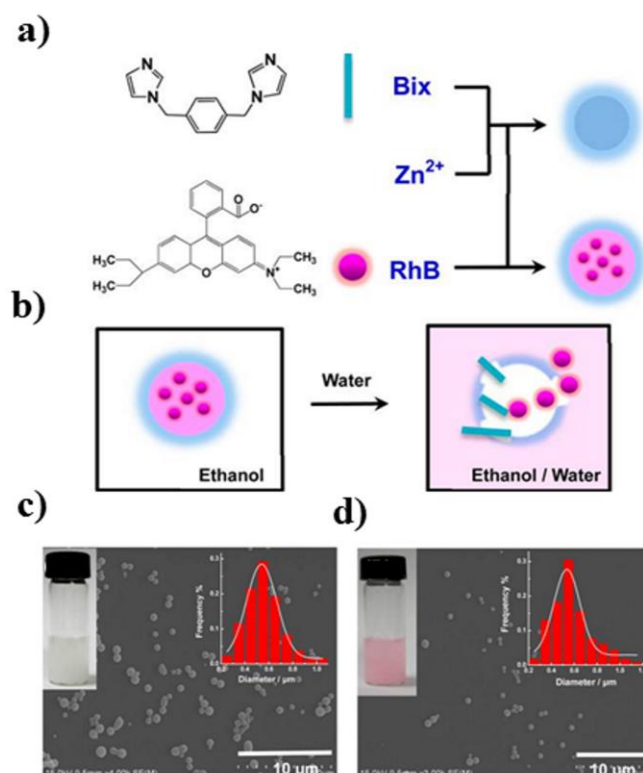


Fig. 28: a) Schematic representation of encapsulation of RhB within the Zn-bix CPP; b) Water responsive release of RhB from Zn-bix CPP; c) SEM image, photograph and size distribution of Zn-bix CPP; d) SEM image, photograph and size distribution of RhB encapsulated Zn-bix CPP. Fig. 28 are reprint from ref. 59 with permission. Copyright 2015, American Chemical Society.

Following these studies, different combinations of **bix** with other ligands were used to build new coordination polymers. One of the earlier examples of CPPs obtained with mixed ligands was reported by our research group in 2008.⁵³ The reaction of aqueous solution of $Co(CH_3COO)_2$ with a mixture of **bix** and a co-ligand namely 3,5-diterbutylcatechol (3,5-dbcac) resulted in a blue solution which was further precipitated as nanosized CPPs by the addition of water. It was possible to control the particles size (from 76 ± 9 nm to 204 ± 13 nm) by changing the rate at addition of water (from 50 to 0.07 mLs⁻¹) in the precipitation step. X-ray powder diffraction data of the resulting material showed that the particles are amorphous which prevented a detailed analysis of the structural connectivity. The elemental analysis of these particles was consistent with the proposed chain formation with formula $[Co(bix)(3,5-dbcac)_2]_n$ (Fig. 29a). The infrared spectra showed that the catechol and bridging **bix** ligands were coordinated to the cobalt ions, as evidenced by the presence of characteristic bands of the ligands involved. However, to provide further evidence for formation of the 1D coordination polymer in the particle-formation process, a model reaction was repeated using a non-flexible ditopic *N,N'* ligand, 4,4'-bipyridyl (4,4'-bipy) instead **bix**. With this modification, it was possible to get single crystals of a polymer with formula $[Co(4,4'-bipy)(3,5-dbcac)_2]_n$ suitable for X-ray diffraction studies. The crystal structure revealed the expected 1D polymer structure, in which metal ions are anchored by four oxygen atoms of the catechol ligands in equatorial positions and two 4,4'-bipy ligands in axial positions (Fig. 29b). This confirms the tendency for bridging N-aromatic N-donor ligands to form chains in these types of polymeric materials. This approximation open new approaches for the design and synthesis of novel functional materials based on metal-organic coordination polymers. Interestingly, this cobalt-based material displays gradual valence-tautomeric interconversion directly related to the electroactive $[Co(3,5-dbcac)]$ units,⁵³ encapsulation

and drug release properties,⁶⁰ and in a very recent work, this same CP was tested as a visual and fluorescent dual probe for hypochlorite (ClO_4^-) sensing based on its stimuli-responsive properties.⁶¹

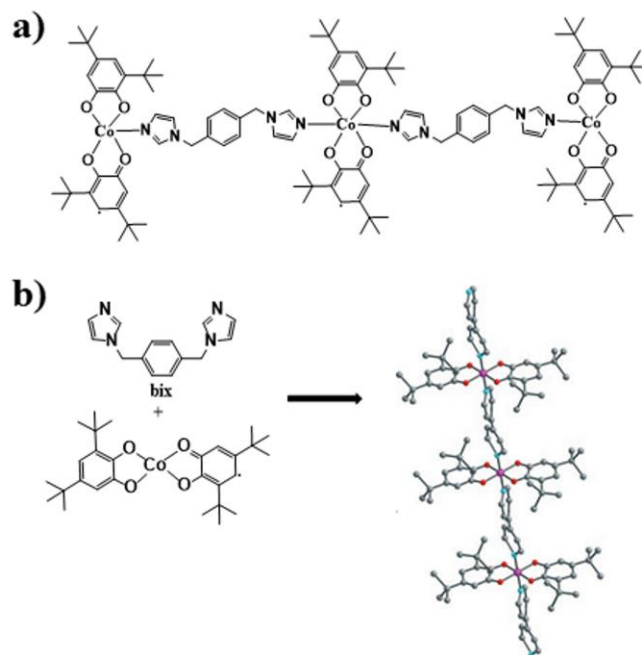


Fig. 29: a) Schematic representation of the proposed structure $[\text{Co}(\text{bix})(3,5\text{-dbcac})_2]_x$; b) Schematic of the synthesis and crystalline structure obtained for $[\text{Co}(4,4'\text{-bipy})(3,5\text{-dbcac})_2]_x$. Fig. 28 are reprint from ref. 53 with permission. Copyright 2008, Wiley-VCH Verlag GmbH & Co. KGaA, Weinheim.

The mixed ligand systems open a wide variety of functional materials in which the combination of **bix** ligand as polymerizing agent and a functional co-ligand offer multiple opportunities to build materials with interesting properties. In this way, various nanosystems based in mixed ligand materials have been synthesized and characterized in our research group. Thus, a bis-catechol ligand having imine backbone also was explored as co-ligand with **bix** for the synthesis of pH sensitive cobalt CPPs. The chemical characterization of this material indicate a bis-catechol:bix:Co ratio close to 1:1:1. However, no structural characterization was possible due to the amorphous nature of the CP. Interestingly the imine functionality showed a pH sensitivity which affects the spin transition properties of the cobalt-based CPPs.⁶² The catechol coligand is a good moiety to introduce novel functionalities on the coordination polymer and to have control over the chemistry of colloid surfaces. For example, the reaction of the carboxyl functionalized catechol 3,4-dihydroxycinnamic acid (dhc) with bix and $\text{M}(\text{CH}_3\text{COO})_2 \cdot x\text{H}_2\text{O}$ metal salts ($\text{M}=\text{Fe}, \text{Co}$) in a 2:1:1 molar ratio generate nanoparticles of around 100 nm. The characterization data were agree with a 1D polymer of general chemical formula $[\text{M}(\text{dhc})_2(\text{bix})]_n$.⁶³ The presence of COOH functionality on the surface of the resulting nanoparticles matrix undergo post synthetic functionalization what offers multiple possibilities to increase its functionality for the theranostic application in nanomedicine. Recently, this previous iron-based CP $[\text{Fe}(\text{dhc})_2(\text{bix})]_n$ was used to encapsulate iron oxide nanoparticle (SPIONS). The SPIONS show a powerful T_2 -negative contrasts agent for MRI, meanwhile the 1D CP showed intrinsic T_1 -positive relativity for MRI what allow to construct a dual T_1/T_2 contrast agent for combination of both entities in a same nanoconstruc. This hybrid material showed an extraordinary improvement in relaxometry and low cytotoxicity in comparison with commercial contrast agents, which make it suitable material for its application as dual contrast agent for MRI.⁶⁴

In another work, **bix** ligand was also combined with a catechol co-ligand having long alkyl chain (4-heptadecylcatechol) and reacted with $\text{Co}(\text{OAc})_2$ resulted in a linear 1D hydrophobic CPP with catechol:bix:Co ratio of 2:1:1, which showed effective separation of oils from water surface through a simple filtration process.⁶⁵

As outlined in the presented examples, CPPs have emerged as a promising platform for developing novel nanomaterials with application in nanomedicine. Their synthetic tenability and reproducibility has allowed the design of a large number of hybrid nanomaterials for cancer therapy, drug delivery, biomedical imaging, and biological sensing. However, more studies are needed to assess the clinical relevance of many of the reported CPPs such as more rigorous in vivo testing, optimization of surface functionalization, and evaluation of “ADME” properties (“absorption-distribution-metabolism-excretion”) to understand their in vivo toxicity profiles. On the basis of the trends observed for other classes of nanomedicines, CPPs are expected to be relevant in anticancer therapeutics or chronic diseases and in clinical imaging than for imaging agents or therapies for chronic indications. Their synthetic tunability allows to fine-tune their properties for biomedical applications as well as to combine multiple therapeutic/imaging modalities into one platform to synergistically enhance therapeutic/diagnostic efficacy.

Intrinsic limitations of amorphous CPs for structural characterization.

As observed, the most developed studies concerning amorphous materials based on exclusively **bix** ligands are focused in Zn-bix derivatives and their use in encapsulation of different active species. Although the enormous potential in different research areas, practically all the studies are addressed to the application of Zn-bix systems to nanomedicine. This material offers encapsulation and optical properties which can be suitable to construct nanomaterials with multifunctional theranostic (therapeutic + diagnostic) properties. However, the difficulty to get structural information from these materials does not allow us to establish a correlation between structure and properties. Thus, the characterization includes size and morphological studies by DLS and electronic microscopies (SEM, TEM). The analysis by X-ray powder diffraction uniquely corroborates the amorphous structure and energy dispersive X-ray (RX-EDS) microanalysis, showed a pseudoquantitative analysis of every sphere elements (i.e. zinc, iron, oxygen, nitrogen, and carbon). IR spectroscopy, and elemental analysis performed on Zn(bix) spheres indicated that they are generated from the coordination polymerization of Zn(II) metal ions connected through **bix** ligands. Furthermore, the chemical composition determined by elemental analysis agrees with the formation of a polymer of formula $[\text{Zn}(\text{bix})(\text{NO}_3)_2]$. If this material is compared with the related crystalline materials **4** and **4a** obtained from the same synthetic methodology, but different metal-to-ligand ratio. Thus, for **4** and **4a** the ratio Zn:bix was 3:1 and 2:1, respectively. Meanwhile, for Zn-bix amorphous material the ratio decreased to 1:1. In basis of the obtaining results, we tentatively can conclude that when the concentration of **bix** is decreasing, the NO_3^- anions enter in the coordination sphere of Zn(II) and promote the generation of a linear 1D Zn-bix coordination polymer with high degree of flexibility in which **bix** ligand is linked the metal ions.

The different CPs described above have been characterized for complementary techniques such as IR, electronic microscopies (SEM, TEM), RX-EDS, NMR, ICP-MS and elemental analysis, which elucidate their chemical composition and indicate the polymeric nature of the related materials. However, the lack of X-Ray diffraction characterization due to their amorphicity and the presence of interstitial ligands, solvents or other species encapsulated limit the structural characterization. It is worth mentioning that differences observed in elemental analysis of different mixed-ligands CP differ slightly from the expected values, a fact that has been tentatively

attributed to the encapsulation of free ligand molecules or solvent molecules within the particles along its formation process, as already reported.⁶⁰

All the examples of amorphous **bix**-based CPPs have been synthesized by room temperature direct precipitation in solution phase. This synthetic methodology normally induces the formation of amorphous materials. Although the resulting materials prevent their structural characterization, the experimental evidences and the characterization studies give us valuable information concerning their physicochemical properties. Their encapsulation properties, facile synthesis, reproducibility, scalability and versatility make them interesting materials for application in different technological fields, from electronics to nanomedicine.

However, a great effort is required to better structural characterization for elucidate the composition/structure of the amorphous solid probes. The comprehensive characterization of amorphous coordination polymers requires a wide gamut of analytical techniques. Thermogravimetric (TGA) and differential scanning calorimetry (DSC) to extract information concerning molecular mobility, possible phase separation, presence of pseudo-crystalline domains, occlusion of solvents, and molecular interactions. Infrared, Raman, and solid-state nuclear magnetic resonance spectroscopy (SS-NMR) analyse the chemical composition and molecular interactions among the components and information about some structural parameters. Scanning/transmission electron microscopy, and atomic force microscopy (AFM) probe the morphological characteristics. Powder X-ray diffraction is selective for detecting/quantifying the crystallinity. Inductively coupled plasma mass spectrometry (ICP-MS) is able to determine with high precision the amount of metal, and other specific techniques such as X-ray photoelectron spectroscopy (XPS), or Mössbauer spectroscopy to know the oxidation state of the metal.

Although the physicochemical properties of these materials were well characterized and offer interesting properties for their use in nanomedicine and in electrical, optical, or magnetic devices, there is a notable limitation in order to know the structural properties of this polymeric materials. So, further studies should be addressed in this sense taking as reference the previous works with related crystalline materials or performing indirect characterization studies with crystalline close models as previously published by us.⁵³

3. Conclusions

The progress and achievements in going from crystalline CPs to amorphous CPs build resulting from the coordination of **bix** with metal salts are emphasized in this perspective. From one hand, crystalline CPs built from **bix** offers not so much applications until date, but the solid state structure characterization of a wide variety of metal-**bix** combinations principally based on Ag(I), Zn(II), Cd(II), Co(II), Cu(II), Fe(II) and Mn(II) metal ions has given us a lot of information concerning the coordination ability and versatility of **bix** ligand. The counter anion nature, the metal-to-ligand ratio, the reaction conditions and the different conformations of the semi-flexible **bix** ligand are key parameters to design and control the synthesis of a determined polymeric architecture. Moreover the supramolecular interactions involving the aromatic and imidazole moiety of the **bix**, the counter anion, or ever the solvent also determine the overall dimensionality and structure of the corresponding CPs. By exploiting the flexible **bix** ligand having *gauche* and *trans* conformations as discussed in this perspective, much progress (in terms of structure) has been made in the field of entanglement (polyrotaxane in **1**, **1a**, **5**, **14** and **18**, polycatenation in **26** and **29**) and interpenetration of coordination polymer (different interpenetration of 2D, 3D CPs **2**, **4a**, **10**, **17** and **30**), but their possible practical applications have not been yet explored. In general, the phenomenon of interpenetration is

considered a disadvantage for the functional CPs, because it blocks the space (voids) in the crystalline CPs. However, these structural particularities can be interesting in future applications such as storage and release of guest species.⁶⁶

The amorphous CPs derived from the coordination of metal ions with **bix** are very scarce due to the intrinsic difficulty to get structural information and its correlation with physicochemical properties. Practically, all the amorphous metal-bix CPs contains Zn(II) because the coordination of this metal ion to **bix** generate materials at the nanoscales with interesting encapsulation properties, fluorescent emission, pH sensitive responses, and high stability and biocompatibility in physiological environments. The supramolecular interactions also play a big role for the interaction and stabilization of guest species and the host CPP matrix; the opportunity of such interactions onto novel applications and improvement of the already reported CPPs such as nano-medicine, useful materials in industry, cosmetics, sensors etc., are the current research interest of coordination chemists. The combination of **bix** with other co-ligands allow to build new material with improved properties and added functionalities in order to obtain multifunctional devices with a wide range of opportunities and application in different technological fields.

The amount of interesting examples listed in this review showed the different parameters which are crucial in the formation, crystallization process, and final architecture/structure of diverse metal-bix combinations. All these experimental results join to crystal engineering concepts bring us closer to a rational understanding of the control of self-assembly properties of **bix** ligand. One of the next steps in the future is to develop novel applications for both crystalline and amorphous coordination polymers using the knowledge obtained from the previous reported materials.

Acknowledgements

NNA thanks EU for Marie Curie Intra-European Fellowship. FN and DRM thanks ICN2-CSIC, Spain for infrastructural and financial support and specially the students and collaborators for their contribution in amorphous CPPs. This work was supported by project MAT2015-70615-R from the Spanish Government and by FEDER funds. ICN2 acknowledges support from the Severo Ochoa Program (MINECO, Grant SEV-2013-0295).

Notes and references

- 1 J.-M. Lehn, *Supramolecular Chemistry—Scope and Perspectives Molecules, Supermolecules, and Molecular Devices (Nobel Lecture)*, *Angew. Chem. Int. Ed.*, 1988, **27**, 89.
- 2 J. W. Steed, D. R. Turner and K. J. Wallace, *Core Concepts in Supramolecular Chemistry and Nanochemistry*, John Wiley & Sons, Ltd, Chichester, UK, 2007.
- 3 (a) K. Ariga, H. Ito, J. P. Hill and H. Tsukube, *Chem. Soc. Rev.*, 2012, **41**, 5800–5835; (b) M. D. Pluth, R. G. Bergman and K. N. Raymond, *Acc. Chem. Res.*, 2009, **42** (10), pp 1650–1659; (c) P. A. Gale, *Acc. Chem. Res.*, 2011, **44** (3), 216–226.
- 4 (a) H.-L. Chen, B. Zhao and Z. Wang, *Journal of Inclusion Phenomena and Macrocyclic Chemistry*, 2006, **56**, 17–21; (b) S. Yuan, Y.-K. Deng and Di Sun, *Chem. Eur. J.* 2014, **20**, 10093–10098; (c) D. Sun, Z.-H. Yan, V. A. Blatov, L. Wan and D.-F. Sun, *Cryst. Growth Des.*, 2013, **13**, 1277–1289; (d) D. Sun, Z.-H. Yan, Y.-K. Deng, S. Yuan, L. Wang and D.-F. Sun, *CrystEngComm*, 2012, **14**, 7856–7860; (e) S. Yuan, H. Wang, D.-X. Wang, H.-F. Lu, S.-Y. Feng and D. Sun, *CrystEngComm*, 2013, **15**, 7792–7802.
- 5 B. F. Abrahams, B. F. Hoskins, R. Robson and D. A. Slizys, *Acta Cryst.* 1998, **C54**, 1666–1668.
- 6 B.-Q. Ma, L. F. Vieira Ferreira and P. Coppens, *Org. Lett.*, 2004, **6**, 1087–1090.
- 7 B.-Q. Ma, Y. Zhang and P. Coppens, *J. Org. Chem.*, 2003, **68**, 9467–9472.
- 8 X.-J. Shen, H.-L. Chen, F. Yu, Y.-C. Zhang, X.-H. Yang and Y.-Z. Li, *Tetrahedron Lett.* 2004, **45**, 6813–6817.
- 9 C. Li, S. Chen, J. Li, K. Han, M. Xu, B. Hu Y. Yu and X. Jia, *Chem. Commun.*, 2011, **47**, 11294–11296.
- 10 C. B. Aakeröy, J. Desper, B. Leonard, and J. F. Urbina, *Cryst. Growth Des.* 2005, **5**, 865–873.
- 11 (a) R. Robson, *J. Chem. Soc., Dalton Trans.*, 2000, 3735–3744; (b) S. R. Batten, S. M. Neville and D. R. Turner, *Coordination Polymers: Design, Analysis and Application*. Cambridge: Royal Society of Chemistry, 2008; (c) C. Janiak, *Dalton Trans.*, 2003, 2781–2804; (d) S. Kitagawa, R. Kitaura and S.-i. Noro, *Angew. Chem. Int. Ed.*, 2004, **43**, 2334–2375.
- 12 (a) P. Kumar, A. Deep and K.-H. Kim, *Trends Anal. Chem.*, 2015, **73**, 39–53; (b) M. Paul, N. N. Adarsh and P. Dastidar, *Cryst. Growth Des.* 2014, **14** (3), 1331–1337; (c) D. Maspoch, D. Ruiz-Molina and J. Veciana, *J. Mater. Chem.*, 2004, **14**, 2713–2723; (d) C. Wang, T. Zhang, and W. Lin, *Chem. Rev.*, 2012, **112**, 1084–1104; (e) Y. Fu, P. Li, L. Bu, T. Wang, Q. Xie, J. Chen and S. Yao, *Anal. Chem.*, 2011, **83**, 6511–6517; (f) D. Liu, R. C. Huxford and W. Lin, *Angew. Chem. Int. Ed.*, 2011, **50**, 3696–3700; (g) L. Wang, Y. Han, X. Feng, J. Zhou, P. Qi and B. Wang, *Coord. Chem. Rev.*, 2016, **307**, 361–381; (h) H. S. Quah, W. Chen, M. K. Schreyer, H. Yang, M. W. Wong, W. Ji and J. J. Vittal, *Nat. Commun.*, 2015, **6**, 7954; (i) S. Banerjee, N. N. Adarsh and P. Dastidar, *Eur. J. Inorg. Chem.* 2010, 3770–3779; (j) J. D. Rocca, D. Liu, and W. Lin, *Acc. Chem. Res.*, 2011, **44**, 957–968; (k) S. Banerjee, N. N. Adarsh and P. Dastidar, *Soft Matter*, 2012, **8**, 7623–7629.
- 13 N. N. Adarsh and P. Dastidar, *Chem. Soc. Rev.*, 2012, **41**, 3039–3060.
- 14 B.-L. Fei, W.-Y. Sun, Y.-A. Zhang, K.-B. Yu and W.-X. Tang, *Dalton Trans.*, 2000, 2345–2348.
- 15 J. Reedijk, *Comprehensive Coordination Chemistry*, Wilkinson, G., Gillard, R.D., McCleverty, J., Eds.; Pergamon: Oxford, 1987; **2**, 76–78.
- 16 F. H. Allen, *Acta Crystallogr., Sect. B: Struct. Sci.*, 2002, **58**, 380.
- 17 CSD, version 5.36 updates (May 2015).
- 18 J. Bruno, J. C. Cole, P. R. Edgington, M. Kessler, C. F. Macrae, P. McCabe, J. Pearson and R. Taylor, *Acta Crystallogr., Sect. B: Struct. Sci.*, 2002, **58**, 389–397.
- 19 B. F. Hoskins, R. Robson and D. A. Slizys, *J. Am. Chem. Soc.*, 1997, **119**, 2952.
- 20 V. A. Blatov and D. M. Proserpio, TOPOS 4.0, *A program package for multipurpose Crystallochemical analysis*.
- 21 Y.-P. Wu, L.-L. Wen, Y.-Z. Li, D.-B. Dang, Z.-D. Lu, Q.-J. Meng and W. H. Xuebao, *Chin. J. Inorg. Chem.*, 2005, **21**, 1759.
- 22 J.-D. Lin, Z.-H. Li, J.-R. Li and S.-W. Du, *Polyhedron*, 2007, **26**, 107.
- 23 L. Chen, J. Ma, Q. Chen, R. Feng, F. Jiang and M. Hong, *Inorg. Chem. Commun.*, 2012, **15**, 208–211.
- 24 B. F. Hoskins, R. Robson and D. A. Slizys, *Angew. Chem. Int. Ed.*, 1997, **36**, 2336–2338.
- 25 S. K. Chawla, M. Arora, K. Nättinen and K. Rissanen, *Mendeleev Commun.* 2006, **16**(2), 89–90.
- 26 L. Carlucci, G. Ciani and D. M. Proserpio, *Crys. Growth Des.*, 2005, **5**, 37–39.
- 27 P. Suresh, C. N. Babu and G. Prabusankar, *Polyhedron*, 2015, **93**, 84–9.
- 28 C. Wang, B. Wen, Z.-Y. Sun, P.-F. Yan and J.-S. Gao, *Acta Crystallogr., Sect. E: Struct. Rep. Online*, 2012, **68**, m621.
- 29 J. Fan, C. Slebodnick, R. Angel and B. E. Hanson, *Inorg. Chem.* 2005, **44**, 552–558.
- 30 J. Fan, C. Slebodnick, D. Troya, R. Angel and B. E. Hanson, *Inorg. Chem.*, 2005, **44**, 2719–2727.
- 31 B. F. Abrahams, B. F. Hoskins, R. Robson and D. A. Slizys, *CrystEngComm*, 2002, **4**(79), 478–482.
- 32 C. N. Babu, P. Suresh, N. Sampath and G. Prabusankar, *J. Mol. Struct.*, 2014, **1075**, 147.
- 33 F.-A. Li, W.-C. Yang and X.-M. Hu, *Z. Kristallogr.-New Cryst. Struct.*, 2011, **226**, 587.
- 34 C. Liu, Y. Yin, X. Shi, D. Zhang and M. Hu, *Inorg. Chem. Commun.*, 2007, **10**, 37–39.
- 35 F.-J. Dan, C. Li, D.-S. Li, Y.-Q. Mu, J.-J. Yang and J. Zhao, *J. Inorg. Organomet. Polym. Mater.*, 2013, **23**, 446.
- 36 L. Carlucci, G. Ciani and D. M. Proserpio, *Chem. Commun.*, 2004, 380–381.
- 37 Q. Zhao, H. Li, X. Wang and Z. Chen, *Chemistry Letters*, 2002, 988–989.
- 38 J. Fan, G. T. Yee, G. Wang, and B. E. Hanson, *Inorg. Chem.*, 2006, **45**, 599–608.
- 39 S. K. Chawla, M. Arora, K. Nättinen, K. Rissanen and J. V. Yakhmi, *Polyhedron*, 2004, **23**, 3007.
- 40 J. Yang, J.-F. Ma, Y.-Y. Liu, J.-C. Ma and S. R. Batten, *Cryst. Growth Des.* 2008, **8**, 4383.
- 41 T. Li, S.-M. Hu, Z.-H. Li, S.-W. Du and J. Huaxue, *Chin. J. Struct. Chem.*, 2006, **25**, 85.
- 42 L. Carlucci, G. Ciani, D. M. Proserpio and L. Spadacini, *CrystEngComm*, 2004, **6**(20), 96–101.
- 43 A. Beheshti, A. Lalegani, G. Bruno, H. A. Rudbari and V. Nobakht, *Inorg. Chim. Acta*, 2013, **408**, 214–221.
- 44 P. Gülich, A. B. Gaspar and Y. Garcia, *Beilstein J. Org. Chem.* 2013, **9**, 342–391.
- 45 L. Carlucci, G. Ciani, S. Maggini, and D. M. Proserpio, *Cryst. Growth Des.* 2008, **8**, 162–165.
- 46 G. R. Desiraju, J. J. Vittal and A. Ramanan, *Crystal Engineering — A Textbook*, World Scientific, 2011.
- 47 M. Oh and C. A. Mirkin, *Nature*, 2005, **438**, 651–654.
- 48 X. Sun, S. Dong and E. Wang, *J. Am. Chem. Soc.*, 2005, **127**, 13102–13103.
- 49 K. H. Park, K. Jang, S. U. Son and D. A. Sweigart, *J. Am. Chem. Soc.*, 2006, **128**, 8740–8741.

- 50 W. J. Rieter, K. M. Pott, K. M. L. Taylor and W. Lin, *J. Am. Chem. Soc.*, 2008, **130**, 11584–11585.
- 51 C. He, D. Liu and W. Lin, *Chem. Rev.*, 2015, **115** (19), 11079–11108.
- 52 E. Coronado, J. R. Galan-Mascaros, M. Monrabal-Capilla, J. Garcia-Martinez and P. Pardo-Ibanez, *Adv. Mater.*, 2007, **19**, 1359.
- 53 I. Imaz, D. Maspoch, C. Rodriguez-Blanco, J. M. Perez-Falcon, J. Campo and D. Ruiz-Molina, *Angew. Chem. Int. Ed.*, 2008, **47**, 1857–1860.
- 54 (a) W. J. Rieter, K. M. L. Taylor, H. An, W. Lin and W. Lin, *J. Am. Chem. Soc.*, 2006, **128**, 9024–9025; (b) K. M. L. Taylor, W. J. Rieter and W. Lin, *J. Am. Chem. Soc.*, 2008, **130**, 14358–14358.
- 55 F. Novio, J. Simmchen, N. Vázquez-Mera, L. Amorín-Ferré and D. Ruiz-Molina, *Coord. Chem. Rev.*, 2013, **257**, 2839–2847.
- 56 I. Imaz, J. Hernando, D. Ruiz-Molina and D. Maspoch, *Angew. Chem. Int. Ed.*, 2009, **48**, 2325–2329.
- 57 I. Imaz, M. Rubio-Martínez, L. García-Fernández, F. García, D. Ruiz-Molina, J. Hernando, V. Puentes and D. Maspoch, *Chem. Commun.*, 2010, **46**, 4737–4739.
- 58 L. Xing, Y. Cao and S. Che, *Chem. Commun.*, 2012, **48**, 5995–5997.
- 59 Jingjing Deng, Wenjie Ma, Ping Yu, and Lanqun Mao, *Anal. Chem.* 2015, **87**, 6958–6965.
- 60 L. Amorín-Ferré, F. Busqué, J. L. Bourdelande, D. Ruiz-Molina, J. Hernando and F. Novio, *Chem. Eur. J.* 2013, **19**, 17508–17516.
- 61 X. Zhang, J. Deng, G. Shib and T. Zhou, *RSC Adv.*, 2015, **5**, 107964–107969.
- 62 F. Nador, F. Novio and D. Ruiz-Molina, *Chem. Commun.*, 2014, **50**, 14570–14572.
- 63 F. Novio, J. Lorenzo, F. Nador, K. Wnuk and D. Ruiz-Molina, *Chem. Eur. J.*, 2014, **20**, 15443–15450.
- 64 M. Borges, S. Yu, A. Laromaine, A. Roig, S. Suárez-García, J. Lorenzo, D. Ruiz-Molina and F. Novio, *RSC Adv.*, 2015, **5**, 86779–86783.
- 65 F. Novio and D. Ruiz-Molina, *RSC Adv.*, 2014, **4**, 15293–15296.
- 66 J. I. Feldblyum, A. G. Wong-Foy and A. J. Matzger, *Chem. Commun.*, 2012, **48**, 9828.